# Inert and seed-competent tau monomers suggest structural origins of aggregation

Hilda Mirbaha[1], Dailu Chen[1], Olga A. Morozova[2], Kiersten M. Ruff[3], Apurwa Sharma[1], Xiaohua Liu[4], Rohit V. Pappu[3], David W. Colby[2], Hamid Mirzaei[4], Lukasz A. Joachimiak[1], Marc I. Diamond[1]

[1]Center for Alzheimer's and Neurodegenerative Diseases, University of Texas, Southwestern Medical Center, Dallas, Texas 75390

[2]Department of Chemical and Biomolecular Engineering, University of Delaware, Newark, Delaware 19716

[3]Department of Biomedical Engineering, Washington University in St. Louis, St. Louis, Missouri 63130

[4]Department of Biochemistry, University of Texas, Southwestern Medical Center, Dallas, Texas 75390

Corresponding Author
Marc I. Diamond, M.D.
NL10.120
5323 Harry Hines Blvd.
Dallas, TX 75390

Email: marc.diamond@utsouthwestern.edu
Phone: 214-648-8857

**Abstract**

Tauopathies feature progressive accumulation of tau amyloids. Pathology may begin when these amplify from a protein template, or seed, whose structure is unknown. We have purified and characterized distinct forms of tau monomer—inert ($M_i$) and seed-competent ($M_s$). Recombinant $M_s$ triggered intracellular tau aggregation, induced tau fibrillization *in vitro*, and self-assembled. $M_s$ from Alzheimer's disease also seeded aggregation and self-assembled *in vitro* to form seed-competent multimers. We used crosslinking with mass spectrometry to probe structural differences in $M_i$ vs. $M_s$. Crosslinks informed models of local peptide structure within the repeat domain which suggest relative inaccessibility of residues that drive aggregation (VQIINK/VQIVYK) in $M_i$, and exposure in $M_s$. Limited proteolysis supported this idea. Although tau monomer has been considered to be natively unstructured, our findings belie this assumption and suggest that initiation of pathological aggregation could begin with conversion of tau monomer from an inert to a seed-competent form.

## Introduction

Amyloids are ordered protein assemblies, typically rich in beta sheet, that underlie multiple disorders such as Alzheimer's disease (AD). Amyloid-forming proteins include tau, synuclein, and expanded polyglutamine proteins such as huntingtin, among many others. It is unknown how or why intracellular proteins such as tau transition from a relatively inert form to one that efficiently self-assembles into ordered structures *in vivo*. This process begins with the formation of a pathogenic "seed," a structure that serves as a template for homotypic fibril growth. This structural transition could be a critical event in the pathogenesis of neurodegeneration. Under defined conditions and relatively high concentrations (typically micromolar), recombinant tau monomer will form amyloid fibrils *in vitro*. However the basis of spontaneous assembly in cells is unknown. The conversion of a protein from a monomer to a large, ordered multimer could occur by several mechanisms, but the first step probably involves the formation of a seed. This event, and indeed the actual conformation or assembly state of the protein that constitutes the "minimal" seed, has remained obscure. This has led to the idea that a seed is potentially transitory, arising from an equilibrium between two states: one relatively aggregation-resistant, and another that is short-lived. A seed could be a single molecule, or several. Based on extrapolation from kinetic aggregation studies, it has been suggested that a critical seed for tau and polyglutamine peptide amyloid formation is a single molecule[1,2], while an earlier study (among others[3]) has proposed a tau multimer[4]. Isolation of the seed-competent form of tau could be critical to understanding the initiation of disease and the design of more effective diagnostics and therapeutics.

Tau forms amyloids that underlie neurodegeneration in a variety of neuropathological syndromes, collectively termed tauopathies[5]. These include AD and frontotemporal dementias, among many others. Multiple groups, including ours, have now observed that tau will propagate an aggregated state from the outside to the inside of a cell, between cells, across synapses, and within brain networks[6]. In prior work we used size exclusion chromatography (SEC) to define tau trimers as the minimal unit of spontaneous cellular uptake and intracellular amyloid formation, and proposed this as the smallest particle capable of propagating aggregates between cells[7]. This work involved application of "naked" protein assemblies derived from recombinant protein or human brain onto cultured "biosensor" HEK293 cells or primary neurons that express a tau aggregation reporter[8,9]. Biosensor cells and primary neurons alike take up tau aggregates via macropinocytosis[10]. The aggregates subsequently serve as highly specific templates to trigger intracellular amyloid formation[9,11]. We have also determined that preincubation of cationic lipids such as Lipofectamine with tau seeds facilitates their direct transduction into a cell, bypassing the physiologic uptake mechanism[9,12]. Lipofectamine-mediated delivery into biosensor cells allows direct quantitation of seed titer for both tau and $\alpha$-synuclein[10].

Tau is intrinsically disordered upon isolation from bacteria or mammalian cells and is relatively inert in terms of spontaneous self-assembly. However under various conditions, including exposure to polyanions such as heparin, tau will form aggregates via nucleated self-assembly [13,14]. It is unknown how these experimental conditions relate to the initiation of aggregation in human brain. We have now purified various stable forms of full-length tau monomer from recombinant sources and human brain. One is relatively inert and is stable for long periods. Another is "seed-competent," triggers amyloid formation in cells and *in vitro*, and exhibits intrinsic properties of self-assembly. We have used crosslinking with mass

spectrometry (XL-MS) to probe the structures of these molecules. Models of discrete regions within the RD predict that differential exposure of hexapeptide motifs previously known to be important for amyloid formation distinguishes the two forms of tau. These models are supported by limited proteolysis studies. The identification of distinct and stable forms of tau monomer, including some that are uniquely seed-competent, bears directly on how we understand the initiation of protein aggregation in the tauopathies.

## MATERIALS AND METHODS

### Tau expression, purification, fibrillization, and labeling

We utilized several forms of recombinant tau. Full-length (FL), wild-type (WT) tau contains two cysteines that create disulfide bridges and could complicate isolation of monomer. Thus in addition to preparing FL WT tau (2N4R) as previously described[15], we purified FL tau (2N4R) that contains two cysteine/alanine substitutions (C291A, C322A), termed tau (2A). We used the 2A and WT forms of tau in our initial studies, before exclusively studying WT. Additionally, for fluorescence correlation spectroscopy (FCS), we engineered a single cysteine at the amino terminus (Cys-Tau (2A)) for labeling via maleimide chemistry. These modified proteins have fibrillization and seeding properties similar to FL WT tau. To initiate fibrillization, we incubated 8μM tau in 10mM HEPES, 100mM NaCl, and 8 μM heparin (1:1 ratio of FL tau to heparin) at 37°C for 72 h without agitation. For cysteine labeling, we incubated 200 μL of 8μM fibrils (monomer equivalent) and monomer with 0.025 mg of Alexa Fluor-488 (AF488) C5-maleimide (Invitrogen) and 80μM Tetramethylrhodamine-5-maleimide (Sigma-Aldrich) overnight at 4°C with gentle rotation. We quenched excess dye with 10mM DTT for 1h at room temperature. For limited heparin exposure, recombinant tau at 1μM was incubated with heparin at 1μM for 15min, 1hr and 4hr at 37°C before purification of monomer via Superdex 200 column.

To avoid confusion throughout the manuscript, we employ the following terminology:

**$M_i$**: This refers to “inert” tau monomer, whether recombinant or derived from control brain.

**$M_s$**: This refers to “seed competent” monomer, whether derived from sonicated fibrils, heparin-treated monomer, or AD brain.

### Sonication and size exclusion chromatography (SEC)

We sonicated labeled and non-labeled fibrils using a Q700 Sonicator (QSonica) at a power of 100-110 watt (Amplitude 50) at 4°C for 3h. Samples were then centrifuged at 10,000 x g for 10 min and 1 mL of supernatant was loaded into a Superdex 200 Increase 10/300 GL column (GE Healthcare) and eluted in PBS buffer at 4°C. After measuring the protein content of each fraction with a Micro BCA assay (Thermo Scientific) and/or fluorescence using a plate reader (Tecan M1000), we aliquoted and stored samples at -80°C or immediately used them in biochemical studies and cell seeding assays. Each aliquot was thawed immediately before use. The molecular weight/radius of proteins in each fraction was estimated by running gel filtration standards (Bio-Rad): Thyroglobulin (bovine) 670 kDa/845nm; γ-globulin (bovine) 158 kDa/5.29nm; Ovalbumin (chicken) 44 kDa/3.05nm; myoglobin (horse) 17 kDa/2.04nm; and vitamin $B_{12}$ 1.35 kDa/0.85nm.

### Size-cutoff filtration

Monomer, dimer and trimer fractions were passed through a 100kDa MWCO filter (Corning) as instructed by the manufacturer (centrifuged at 15,000 x g for 15min at 4°C). Filtered

140 material was immediately collected and used in seeding assay along with the non-filtered
141 samples of the same fraction at a final concentration of 100nM, or analyzed by limited
142 proteolysis. Protein concentration was determined before and after filtration by determining
143 absorption at 205nm.
144
145 **CD spectroscopy**
146 Circular dichroism (CD) measurements were performed at 25°C on a Jasco J-815
147 spectropolarimeter using a 0.1cm optical path length. 200µL of 2µM $M_s$ or $M_i$ monomer was
148 dialyzed onto 10 mM NaP and the spectra were measured at 0.10 nm intervals, with a band
149 width of 1.0nm, and scan speed of 10nm/min. The spectrum represents the average of 4
150 scans in the range of 195 to 250nm.
151
152 **Enzyme-linked immunosorbent assay**
153 A total tau "sandwich" ELISA was performed similarly to that described previously[16].
154 Antibodies were kindly provided by Dr. Peter Davies (Albert Einstein College of Medicine).
155 96-well round-bottom plates (Corning) were coated for 48 hours at 4°C with DA-31 (aa 150-
156 190) diluted in sodium bicarbonate buffer (6µg/mL). Plates were rinsed with PBS 3 times,
157 blocked for 2h at room temperature with Starting Block (Pierce), and rinsed with PBS 5
158 additional times. SEC fractions were diluted in SuperBlock solution (Pierce; 20% SuperBlock,
159 diluted in TBS), and 50 µL sample was added per well. DA-9 (aa 102-150) was conjugated to
160 HRP using the Lighting-Link HRP Conjugation Kit (Innova Biosciences), diluted 1:50 in
161 SuperBlock solution, and 50µL was added per well (15µg/mL). Sample + detection antibody
162 complexes were incubated overnight at 4°C. Plates were washed with PBS 9 times with a 15
163 sec incubation between each wash, and 75 µL 1-Step Ultra TMB Substrate Solution (Pierce)
164 was added. Plates were developed for 30min, and the reaction quenched with 2M sulfuric
165 acid. Absorbance was measured at 450nm using an Epoch plate reader (BioTek). Each plate
166 contained a standard curve, and all samples were run in triplicate.
167
168 **Fluorescence correlation spectroscopy**
169 FCS measurements were conducted on a Confocal/Multiphoton Zeiss LSM780 Inverted
170 microscope (Carl Zeiss-Evotec, Jena, Germany), using a 40X water immersion objective as
171 previously described [17]. Fluorescently labeled tau from SEC fractions (in PBS) was excited at
172 488nm and 561nm for 30sec, recording 10 times[18]. The data analysis was performed with
173 Origin 7.0 (OriginLab, Northampton, MA).
174
175 **Liposome-mediated transduction of tau seeds**
176 Stable cell lines were plated at a density of 35,000 cells per well in a 96-well plate. After 18h,
177 at 60% confluency, cells were transduced with protein seeds. Transduction complexes were
178 made by combining [8.75µL Opti-MEM (Gibco) +1.25µL Lipofectamine 2000 (Invitrogen)] with
179 [Opti-MEM + proteopathic seeds] for a total volume of 20µL per well. Liposome preparations
180 were incubated at room temperature for 20min before adding to cells. Cells were incubated
181 with transduction complexes for 24h.
182
183 **FRET flow cytometry**
184 Cells were harvested with 0.05% trypsin and fixed in 2% paraformaldehyde (Electron
185 Microscopy Services) for 10min, then resuspended in flow cytometry buffer. The MACSQuant
186 VYB (Miltenyi) was used to perform FRET flow cytometry. To measure CFP and FRET, cells
187 were excited with a 405nm laser, and fluorescence was captured with 405/50nm and
188 525/50nm filters, respectively. To measure YFP, cells were excited with a 488nm laser and

189 fluorescence was captured with a 525/50nm filter. To quantify FRET, we used a gating
190 strategy similar to that previously described[9]. The integrated FRET density (IFD), defined as
191 the percentage of FRET-positive cells multiplied by the median fluorescence intensity of
192 FRET-positive cells, was used for all analyses. For each experiment, ~20,000 cells were
193 analyzed in triplicate. Analysis was performed using FlowJo v10 software (Treestar).
194
195 **Tau seeding *in vitro***
196 Recombinant full length (0N4R) tau monomer was purified as previously described[19] at
197 1mg/mL in BRB80 buffer (80mM PIPES, 1mM MgCl2, 1mM EGTA, pH 6.8 with 0.3M NaCl)
198 and boiled at 100°C for 5min with 25mM β-mercaptoethanol. The tau protein solution was
199 then rapidly diluted 1:5 and cooled to 20°C in PBS, pH 7.4, to a final concentration of
200 0.2mg/mL of tau and 5mM β-mercaptoethanol. This solution was supplemented with
201 Thioflavin T (ThT) to a final concentration of 20μM and filtered through a sterile 0.2μm filter.
202 Reaction sizes of 195μL were aliquoted from the prepared protein stock and thoroughly
203 mixed with 5μL of each sample at 100nM monomer equivalent, or 5μL of buffer control. For
204 each sample, three different technical replicates were prepared. An opaque 96-well plate was
205 prepared with a 3mm glass bead added to each well to increase agitation. The recombinant
206 tau solution was added to the plate in 200μl reaction volumes. The plate was sealed with
207 sealing tape to prevent evaporation and incubated in the plate reader (SpectraMax M2) at
208 37°C. ThT fluorescence was monitored over time with excitation and emission filters set to
209 444nm and 485nm, respectively. Fluorescence readings were taken every 5min, with
210 agitation for 5sec before each reading.
211
212 **Tau extraction from brain and characterization by SEC**
213 0.5g frontal lobe sections from AD patients at late Braak stage (VI) and age-matched controls
214 lacking evident tau pathology were gently homogenized at 4°C in 5mL of TBS buffer
215 containing protease inhibitor cocktails (Roche) using a dounce homogenizer. Samples were
216 centrifuged at 21,000 x g for 15 min at 4°C to remove cellular debris. Supernatant was
217 partitioned into aliquots, snap frozen and stored at -80°C. Immunopurification was performed
218 with HJ8.5 anti-tau antibody[20] at a ratio of 1:50 (1μg mAb per 50μg of total protein),
219 incubating overnight at 4°C while rotating. To each 1mL of mAb/brain homogenate we added
220 200μL of a 50% slurry protein G-agarose beads (Santa-Cruz). We washed the bead with TBS
221 buffer before overnight incubation at 4°C. We then centrifuged the complexes at 1000 x g for
222 3min and discarded the supernatant. Beads were washed with Ag/Ab Binding Buffer, pH 8.0
223 (Thermo Scientific) three times. Tau bound to the beads was eluted in 100 μL low pH elution
224 buffer (Thermo Scientific), incubated at room temperature for 7min, followed by neutralization
225 with 10μL Tris-base pH 8.5. This elution step was repeated once more with 50 μL elution
226 buffer and 5μL Tris-base pH 8.5 for a total of 165μL. Samples were then centrifuged at
227 10,000 x g for 10min, and the supernatant loaded onto a Superdex 200 Increase 10/300 GL
228 column (GE Healthcare). SEC fractions were frozen at -80°C after evaluation of protein
229 content by Micro BCA assay (Thermo Scientific).
230
231 To compare different extraction methods, fresh frozen frontal lobe section from an AD patient
232 brain was suspended in TBS buffer containing protease inhibitor cocktails (Roche) at 10%
233 w/vol in 4 portions. Samples were homogenized using 3 different devices: a dounce
234 homogenizer, probe sonicator (Omni International), and tissue homogenizer (Power Gen 125,
235 Fischer Scientific). We also included one more condition of homogenizing with tissue
236 homogenizer followed by probe sonication for 10min. Samples were centrifuged at 21,000 x g

for 15min at 4°C to remove cellular debris. Supernatant was partitioned into aliquots followed by immunopurification.

To control for release of tau $M_s$ from fibrils in AD brain, a tau KO Mouse brain was divided into two halves, followed by spiking one half with recombinant fibrils and the other with fibril-derived $M_s$, both at final concentration of 10μM monomer equivalent. Each was dounce homogenized, centrifuged, immunoprecipitated with HJ8.5 anti-tau antibody, and fractionated by SEC with identical techniques as used for human brain processing. SEC fractions were then used in seeding experiments.

**Analysis of heat denaturation data**

We analyzed the IFD from measurements of temperature dependent seeding using global fits to a proposed unimolecular heat denaturation reaction. This analysis rests on the Arrhenius equation[21]:

$$k_U = Ae^{-\frac{E}{RT}}$$

where $k_U$ is the unfolding rate constant, $E$ is the activation energy, $R$ is the gas constant, $T$ is the temperature, and $A$ is the pre-exponential factor. For the unimodal model, the data were fit globally to:

$$\mathrm{IFD}(t) = 100e^{-t/\tau}.$$

Here, $t$ is the heat denaturation time and $\tau = 1/k_U$ is the unfolding time. A second, multimodal model was deployed to account for discrepancies in the early time points which appeared to suggest the presence of a lag phase in denaturation. In this model, the data were fit globally to

$$\mathrm{IFD}(t) = 100; \qquad t \leq l_t$$
$$\mathrm{IFD}(t) = 100e^{-(t-l_t)/\tau}; t > l_t$$

where $l_t$ is the lag time given by

$$1/l_t = Be^{-\frac{E}{RT}}$$

and $B$ is a pre-exponential factor. We used the Akaike information criterion (AIC) to evaluate the best model as it quantifies the trade-off between goodness of fit and the complexity of the model [22]. For least squares model fitting, AIC can be reduced to:

$$\mathrm{AIC} = 2p + n\ln(\mathrm{RSS}/n)$$

where $p$ is the number of parameters in the model, $n$ is the number of observations, and RSS is the residual sum of squares. The preferred model is the one with the minimum AIC. Here, we find AIC = 123 for the unimodal model and AIC = 105 for the multimodal model, which suggests the multimodal model is a better description of the denaturation data.

**Crosslinking, sample processing and LC-MS/MS analysis**

$M_i$ and $M_s$ tau samples were prepared as described above. In all cases, tau preparations were crosslinked at a total protein concentration of ~0.1mg/mL using 10 – 20μg starting material. The crosslinking buffer was 50 mM HEPES-KOH (pH 7.4) containing 150mM NaCl and 1mM DTT. The crosslinking reaction was initiated by adding disuccinimidyl suberate

284 (DSS) stock solution (25 mM DSS-$d_0$ and –$d_{12}$, Creative Molecules) in DMF to a final
285 concentration of 1mM. Samples were incubated at 37°C for 1min. For the heparin-derived $M_s$
286 sample, heparin sulfate (Sigma) was added to a final concentration of 5µM, followed by 1mM
287 DSS and the samples were incubated for 1min at 37°C. Excess reagent was quenched by
288 addition of ammonium hydrogen carbonate to 50mM and incubation at 37°C for 30min, and
289 then flash frozen at -80°C. Absence of higher molecular species was confirmed by SDS-
290 PAGE and coomassie stain. After the quenching step, samples were evaporated to dryness
291 in a vacuum centrifuge and resuspended in 8M urea. Proteins were reduced with 2.5mM
292 TCEP (37°C, 30 min) and alkylated with 5mM iodoacetamide (30min, room temperature,
293 protected from light). The sample solutions were diluted to 1M urea with 50mM ammonium
294 hydrogen carbonate and trypsin (Promega) was added at an enzyme-to-substrate ratio of
295 1:50. Proteolysis was carried out at 37°C overnight followed by acidification with formic acid
296 to 2% (v/v). Samples were then purified by solid-phase extraction using Sep-Pak tC18
297 cartridges (Waters) according to standard protocols. Samples were fractionated by size
298 exclusion chromatography (SEC) on a Superdex Peptide column as described elsewhere [23].
299 Two fractions collected from SEC were evaporated to dryness and reconstituted in
300 water/acetonitrile/formic acid (95:5:0.1, v/v/v) to a final concentration of approximately 0.5
301 µg/µl. 2µL each were injected for duplicate LC-MS/MS analyses on an Eksigent 1D-NanoLC-
302 Ultra HPLC system coupled to a Thermo Orbitrap Fusion Tribrid system. Peptides were
303 separated on self-packed New Objective PicoFrit columns (11cm x 0.075mm I.D.) containing
304 Magic $C_{18}$ material (Michrom, 3µm particle size, 200Å pore size) at a flow rate of 300nL/min
305 using the following gradient. 0-5min = 5 %B, 5-95min = 5-35 %B, 95-97min = 35-95 %B and
306 97-107min = 95 %B, where A = (water/acetonitrile/formic acid, 97:3:0.1) and B =
307 (acetonitrile/water/formic acid, 97:3:0.1). The mass spectrometer was operated in data-
308 dependent mode by selecting the five most abundant precursor ions (m/z 350-1600, charge
309 state 3+ and above) from a preview scan and subjecting them to collision-induced
310 dissociation (normalized collision energy = 35%, 30ms activation). Fragment ions were
311 detected at low resolution in the linear ion trap. Dynamic exclusion was enabled (repeat count
312 1, exclusion duration 30sec).
313
314 **Analysis of mass spectrometry data**
315 Thermo .raw files were converted into the open .mzXML format using msconvert
316 (proteowizard.sourceforge.net) and analyzed using an in-house version of xQuest[24]. Spectral
317 pairs with a precursor mass difference of 12.075321 Da were extracted and searched against
318 the respective FASTA databases containing Tau (TAU_HUMAN P10636-8). xQuest settings
319 were as follows: Maximum number of missed cleavages (excluding the crosslinking site) = 2,
320 peptide length = 5-50 aa, fixed modifications = carbamidomethyl-Cys (mass shift = 57.021460
321 Da), mass shift of the light crosslinker = 138.068080 Da, mass shift of mono-links =
322 156.078644 and 155.096428 Da, $MS^1$ tolerance = 10 ppm, $MS^2$ tolerance = 0.2 Da for
323 common ions and 0.3 Da for crosslink ions, search in ion-tag mode. For brain-derived
324 samples we also included variable modifications including: Methionine oxidation = 15.99491,
325 Ser/Thr/Tyr Phosphorylation = 79.96633 and Lysine Ubiquitylation = 114.043 with
326 nvariable_mod = 1. Post-search manual validation and filtering of the recombinant samples
327 was performed using the following criteria: xQuest score > 16, mass error between -4 and
328 +7ppm, %TIC > 10, and a minimum peptide length of six aa. In addition, at least four
329 assigned fragment ions (or at least three contiguous fragments) were required on each of the
330 two peptides in a crosslink. False discovery rates (FDR) for the identified crosslinks were
331 estimated using xprophet[24]. For the recombinant samples, $M_i$ and $M_s$, the FDR ranged from
332 6-10%. Post-search manual validation of the brain-derived samples was performed using the

333 following criteria: xQuest score > 7, mass error between -5 and +7ppm, %TIC > 10, and a
334 minimum peptide length of six aa. In addition, at least four assigned fragment ions (or at least
335 three contiguous fragments) were required on each of the two peptides in a crosslink. The
336 FDRs for the brain samples were much higher and ranged between 20-25%. For triplicate
337 datasets corresponding to the $M_i$ and $M_s$ boiling time course we computed consensus
338 crosslink profiles enforcing that at least two of the three datasets contain a crosslink.
339 Crosslink data was visualized using Xvis[25]. Average contact distance was computed by
340 averaging the sequence separation between crosslink pairs in a given dataset.
341
342 **Generation of structural models using XL-MS-derived constraints**
343 High confidence crosslink pairs identified above were used to generate an ensemble of
344 possible structures using a Rosetta protocol employing the crosslink pairs as structural
345 restraints. The integration of XL-MS derived restraints have been previously used to refine
346 structural models of large complexes[23] and simpler heterodimeric complexes[26]. Based on
347 distance distributions of crosslink pairs mapped onto crystallographic structures we set a
348 lower bound of 15Å and an upper bound of 25Å for lysine $C\alpha$ pairs in our simulations.
349 Importantly, in our simulations we weighted the constraint pairs as to allow some distances
350 above the upper bound limit. The fragment library was supplanted by using chemical shifts
351 derived from fibrillar tau ssNMR assignments (bmrb entry 17920) using csrosetta[27]. We
352 generated 1000 models for each of the four XL-MS datasets on a high performance cluster
353 (biohpc.swmed.edu). Representative structures were selected according to the low Rosetta
354 score and radius of gyration. All plots were generated with gnuplot. All figures were
355 generated using Pymol.
356
357 **Commandline used for *ab initio* protocol calculations with XL-MS restraints**
358 AbinitioRelax.default.linuxgccrelease -in:file:fasta tau.fasta -file:frag3 tau.frags3.dat -file:frag9
359 tau.frags9.dat -nstruct 1000 -abinitio::increase_cycles 0.5 -abinitio::relax -score::weights
360 score13_env_hb -abinitio::rg_reweight 0.5 -abinitio::rsd_wt_helix 0.5 -abinitio::rsd_wt_loop
361 0.5 -disable_co_filter true -out:file:silent csrosetta.out -constraints:cst_fa_file tau.cst -
362 constraints:cst_file tau.cst -constraints:cst_weight 0.1 -constraints:cst_fa_weight 0.1 -
363 loopfcst::coord_cst_weight 10.0
364
365 **Statistical analysis**
366 Group mean values were analyzed by one-way ANOVA with Bonferroni post hoc significant
367 differences test using GraphPad prism 5 software. Data in text and figures are represented
368 as mean ± SEM.
369
370 **Kinetic analyses of $M_i$ and $M_s$ proteolysis**
371 Limited proteolysis of $M_i$/$M_s$ using trypsin was carried out in 50mM TEAB at 25 °C. The
372 enzyme to tau ratio was adjusted to 1:100 (wt/wt) with around 11ug of $M_i$/$M_s$ present initially.
373 The total reaction mixture volume was 60µl. Aliquots were withdrawn from the reaction
374 mixture at 1, 5, 15, 30, 60 and 120min by using 10µL of 10% trifluoroacetic acid (TFA) to
375 quench the reaction (PH<3). The trypsin-digested peptides were then desalted using an
376 Oasis HLB plate (Waters) and eluted with 100µL 80% acetonitrile (ACN) containing 0.1%
377 TFA. The solvent was evaporated in a SpeedVac concentrator and the dried samples were
378 reconstituted in 20µl of 2% acetonitrile, 0.1% TFA and 2µl solution was used for by
379 LC/MS/MS analysis, the analysis were performed on an Orbitrap Elite mass spectrometer
380 (Thermo Electron) coupled to an Ultimate 3000 RSLC-Nano liquid chromatography systems

381 (Dionex). Samples were injected onto a 75µm i.d., 15-cm long EasySpray column (Thermo),
382 and eluted with a gradient from 1-28% buffer B over 60 min. Buffer A contained 2% (v/v) ACN
383 and 0.1% formic acid in water, and buffer B contained 80% (v/v) ACN, 10% (v/v)
384 trifluoroethanol, and 0.1% formic acid in water. The mass spectrometer operated in positive
385 ion mode with a source voltage of 2.8kV and an ion transfer tube temperature of 275 °C. MS
386 scans were acquired at 240,000 resolution in the Orbitrap and up to 14 MS/MS spectra were
387 obtained in the ion trap for each full spectrum acquired using collision-induced dissociation
388 (CID), with charge 1 ions rejected. Dynamic exclusion was set for 15s after an ion was
389 selected for fragmentation. Raw MS data files were searched against the appropriate protein
390 database from Uniprot, and reversed decoy sequences appended (Elias and Gygi, 2007) by
391 using Protein Discovery 2.2 (Thermo Fisher Scientific). Fragment and precursor tolerances of
392 20ppm and 0.6Da were specified, and 12 missed cleavages were allowed.
393 Carbamidomethylation of Cys was set as a fixed modification and oxidation of Met was set as
394 a variable modification. Label-free quantitation of proteins across samples was performed.
395 Average peptide intensity values were computed for all time points for each peptide. To
396 estimate differences in kinetic profiles we calculated the median value of each profile and
397 compared the $M_i$ to $M_s$ ratio.
398
399
400 RESULTS
401
402 **Isolation of fibril-derived monomer and other assemblies**
403 We initially sought to define the tau seeding unit that would trigger intracellular aggregation
404 upon direct delivery to the cell interior. We had previously observed that a tau trimer is the
405 minimal assembly size that triggers endocytosis and intracellular seeding[7]. These
406 experiments depended on spontaneous cell uptake, since no Lipofectamine was added to the
407 reactions. A prior study had also indicated the role of disulfide linkages in promoting tau
408 aggregation, potentially by dimer formation[4]. Thus, for our initial studies we engineered and
409 purified full-length (FL) tau monomer that lacks any internal cysteines due to alanine
410 substitutions (C299A and C322A), termed tau (2A). FL tau (2A) cannot self-associate based
411 on disulfide linkages, which helped prevent the formation of cryptic dimers that could have
412 confounded our studies. These substitutions did not affect tau purification, heparin-induced
413 fibrillization, and sonication protocols, which we performed as described previously[7]. We
414 covalently labeled the fibril preps prior to sonication and isolation of recombinant FL tau (2A)
415 assemblies of various sizes by size exclusion chromatography (SEC)[7]. In parallel, we also
416 studied FL wild type (WT) tau. We purified unfibrillized recombinant FL tau (2A) monomer by
417 SEC (Fig. 1A), and isolated SEC fractions of sonicated fibrils that contained putative
418 monomer, dimer, trimer and ~10-mer (Fig. 1B).
419
420 **Fibril-derived monomer exhibits seeding activity in cells and *in vitro***
421 To test the seeding activity of the tau preparations, we used a previously described
422 "biosensor" cell reporter line[9].These cells stably express 4R tau repeat domain (RD)
423 containing the disease-associated P301S mutation, fused to cyan and yellow fluorescent
424 proteins (RD-CFP/YFP). Exogenously applied seeds induce intracellular aggregation with
425 resultant fluorescence resonance energy transfer (FRET) that can be measured via flow
426 cytometry[9,12]. The degree of aggregation is scored using "integrated FRET density" (IFD),
427 which is the product of the percent positive cells and the mean fluorescence intensity of
428 FRET-positive cells, and from this we determine a titer of tau seeding activity[9]. Lipofectamine
429 directly transduces tau assemblies across the plasma membrane and increases the assay's

430 sensitivity by approximately 100-fold. Upon incubation with Lipofectamine, we were surprised
431 to observe seeding by monomer and larger assemblies alike, whether FL WT or 2A. (Fig.
432 1C,D). Epifluorescence microscopy confirmed the presence of intracellular inclusions after FL
433 WT tau monomer seeding (Fig. 1D). We termed the inert monomer "$M_i$," and the seed-
434 competent monomer "$M_s$." To rule out higher order assemblies of tau within the putative
435 monomer fraction, immediately prior to the seeding assay we passed fractions through a
436 100kDa cutoff filter to eliminate anything larger than a monomer. While monomer fraction
437 retained ~80% of seeding activity, only ~20% of dimer seeding activity remained, and ~1-2%
438 of trimer seeding activity remained (Fig. 1E). To exclude an artifact related to Lipofectamine
439 transduction into cells, we tested FL (2A) tau preparations in an *in vitro* seeding assay that
440 induces fibril formation by full-length tau (0N4R) through iterative polymerization and agitation
441 steps[19]. $M_i$ had no intrinsic seeding activity. However $M_s$ induced amyloid formation, albeit
442 more slowly than trimer or unfractionated fibrils (Fig. 1F). This slow aggregation process may
443 reflect inefficient fibril assembly, and a predominance of small nucleated assembly events
444 from the added monomer. We concluded that the $M_s$ fraction contained seeding activity that
445 enabled intracellular aggregation of tau RD-CFP/YFP in cells, or full-length tau *in vitro*.
446 Finally, we tested whether contamination of very small amounts of seeds could somehow
447 account for the seeding activity in monomer fractions by carrying out dose-response titrations
448 of the various preparations. $M_s$ had an $EC_{50}$ of ~10nM (Fig. 1G), which was very similar to
449 dimer and trimer (Fig. 1H). Thus to account for signal observed in the seeding assay,
450 contamination of an otherwise inert monomer with larger seed-competent assemblies would
451 have to be substantial.
452
453 **Comparison of $M_i$ and $M_s$ by CD and FCS**
454 We tested for obvious structural differences between $M_i$ and $M_s$ using CD spectroscopy,
455 which revealed none (Fig. 2A). We re-tested the assemblies using fluorescence correlation
456 spectroscopy (FCS), which measures particle diffusion through a fixed volume. As we
457 previously observed[7], we accurately estimated the units of small assemblies (≤10-mer), but
458 not larger assemblies (>10-mer) (Fig. 2B). In an additional effort to detect cryptic multimers
459 within the $M_s$ preparation, we used double-label FCS. We engineered a cysteine onto the
460 amino terminus of FL tau (2A) to enable its covalent modification (Cys-Tau (2A)). We then
461 prepared Cys-tau (2A) fibrils, or monomer, and labeled them simultaneously with Alexa488
462 (green) and tetramethylrhodamine (TMR) via maleimide chemistry. We carried out sonication
463 and purification by SEC as before, isolating assemblies of various sizes. We evaluated each
464 for cross-correlation between red and green signal, which indicates the presence of at least
465 two tau molecules in a particle. We analyzed >300 events for each assembly. When we
466 evaluated $M_i$ and $M_s$, 100% of events in each case showed a diffusion time consistent with a
467 tau monomer (Fig. 2C,D). Furthermore, we observed no cross-correlation between red and
468 green signal, indicating that neither preparation had detectable multimeric assemblies (Fig.
469 2C,D,H). By contrast, when we evaluated larger species such as dimer, trimer, or ~10-mer,
470 we observed longer diffusion times consistent with the predicted assembly sizes, and
471 significant cross-correlation values (Fig. 2E-H), consistent with the presence of multimers.
472 The FCS studies supported the conclusion that $M_i$ and $M_s$ are comprised predominantly of
473 monomer.
474
475 **SEC preparation efficiently purifies $M_s$ monomer**
476 To rule out cross-contamination of assemblies within the SEC column, we tested its ability to
477 exclude larger seeds from the monomer fraction. We first isolated $M_s$ and larger assemblies
478 from a sonicated fibril preparation (Fig. 3, Group 1). Removing the fraction that contained $M_s$

479 (B5), we then pooled the remaining fractions, and spiked them with $M_i$. We re-fractionated the
480 material on SEC to isolate the monomer in fraction B5 again (Fig. 3, Group 2). As previously
481 observed, $M_s$ and other fibril-derived assemblies in Group 1 had seeding activity (Fig. 3).
482 However, in Group 2, while we observed seeding activity in larger assemblies, the monomer
483 (which we take to be $M_i$) re-isolated from a pool of larger fibril-derived assemblies had no
484 seeding activity (Fig. 3). This confirmed that larger, seed-competent assemblies do not
485 appreciably contaminate the monomer fraction during SEC.
486
487 **Heat denaturation of assemblies**
488 Although prior controls had essentially excluded the presence of tau multimers in the sample,
489 we used heat-mediated dissociation of oligomeric assemblies as an additional test for the
490 possibility that $M_s$ in fact represents a uniquely compact multimer that somehow purifies as a
491 monomer. We collected $M_s$ by SEC, and heated the sample to 95°C for 3h. We then re-
492 isolated the sample via SEC. We carried out the same procedure with trimer and ~20-mer. In
493 each case, we tested the resultant fractions for seeding activity. In the first instance, after
494 heating we re-isolated $M_s$ purely as monomer that retained virtually all of its seeding activity
495 (Fig. 4A). The trimer assembly (fraction B8) broke down to smaller assemblies, predominantly
496 monomer, each of which retained seeding activity (Fig. 4B). The ~20-mer (fraction A5) was
497 largely stable following heat treatment, and retained its seeding activity (Fig. 4C). These
498 experiments highlighted the lability of small multimers (i.e. trimer), and a surprising
499 persistence of seeding activity in heat-treated monomer.
500
501 **Differential heat lability of tau assemblies**
502 In the preceding experiment $M_s$ retained seeding activity even after 3h at 95°C, a condition
503 sufficient to dissociate trimers. These experiments implied that $M_s$ consists of a stable seed-
504 competent structure, resistant to heat denaturation. Consequently, we used more nuanced
505 heat denaturation of seeding activity to probe the relative stabilities of $M_s$, dimer, trimer, and
506 larger assemblies of FL WT tau. We first isolated tau monomer, dimer, trimer, ~10-mer, and
507 ~20-mer on SEC. We then incubated the various assemblies at a range of temperatures (65,
508 75, 85, 95°C) and times (0, 3, 12, 18, 24, 48, 72h) before measuring seeding activity. Lower
509 temperatures only slightly reduced seeding activity, whereas exposure of $M_s$, dimer, and
510 trimer to temperatures ≥85°C for 18-24h eliminated it at roughly the same rate for each (Fig.
511 4D-G). By contrast, the seeding activities of ~10-mer and ~20-mer were relatively heat-
512 resistant (Fig. 4D-G). This was consistent with our prior observations that tau seeds derived
513 from cultured cells are resistant to boiling [11]. To determine a putative energy barrier between
514 $M_s$ and $M_i$, we evaluated the denaturation data for $M_s$ by integrating the data from the prior
515 experiments (Fig. 4H). We compared two models for the transition of $M_s$ to an inert form
516 (which we assumed to be an unfolding reaction): a unimodal unfolding model vs. a
517 multimodal model that assumes intermediate seed-competent states. The unimodal model
518 did not account for the data at early time points, which indicated a lag phase in denaturation,
519 whereas the multimodel model performed better (Fig. 4H). The lag phase in denaturation
520 implied an ensemble of seed-competent states that define $M_s$, each separated by smaller
521 energy barriers. Using the multimodal model, we calculated the barrier to conversion of $M_s$ to
522 an inert form to be ~78 kcal/mol.
523
524 **$M_s$ has unique properties of self-assembly**
525 Aggregation of $M_i$ *in vitro* is relatively slow, requires high protein concentration (micromolar),
526 and polyanions such as heparin[13,14]. Based on the seeding activity of $M_s$ we predicted that it
527 might more readily self-associate. We incubated FL WT tau $M_i$ and $M_s$ alone, or dimer or

528 trimer at equimolar ratios, keeping total particle concentration constant at 500nM. We then
529 monitored change in assembly size over 24h. $M_i$, dimer, and trimer showed no evidence of
530 self-association in this timeframe (Fig. 5A,C,D). By contrast, when incubated alone, $M_s$
531 readily formed larger assemblies (Fig. 5B). When we incubated $M_i$ with dimer or trimer, we
532 saw no change in the assembly population over 24h (Fig. 5E,F). By contrast, when we mixed
533 $M_s$ with dimer or trimer we observed a growth of larger assemblies with a concomitant
534 reduction in dimer and trimer peaks (Fig. 5G,H). We conclude that $M_i$, dimer, and trimer do
535 not form larger assemblies at an appreciable rate, while $M_s$ self-assembles and adds on to
536 larger assemblies.
537
538 **Heparin induces transition from $M_i$ to $M_s$**
539 The preparation of $M_s$ based on sonication of fibrils raised two important issues. First, it left
540 uncertain whether $M_i$ could be converted to a seed-competent form without previously being
541 incorporated into a fibril. Second, we observed that sonication could create fragments from
542 tau monomer that might potentially act as seeds (Supp. Fig. S6A). Consequently, we used
543 heparin to induce the formation of $M_s$, thereby avoiding sonication. We exposed FL WT tau to
544 heparin for varying amounts of time before purifying different assembly sizes by SEC and
545 testing for seeding activity. After 15min of heparin exposure, we detected low but significant
546 amounts of seed-competent monomer, and much fewer larger assemblies (Fig. 6A).
547 Crosslinking of purified, heparin-induced $M_s$ revealed no evidence of multimers or an
548 increase in fragments (Supp. Fig. S6B). Recombinant monomer not treated with heparin had
549 no seeding activity at any time point (Fig. 6A). At longer heparin treatment times (1h, 4h)
550 monomer fractions as well as larger assemblies all had strong seeding activity (Fig. 6A). $M_s$
551 derived from heparin exposure was relatively resistant to heat denaturation at 95°C, albeit
552 less so than fibril-derived $M_s$ (Fig. 6B). Relative seeding efficiency of the various forms of $M_s$
553 as well as sonicated or unsonicated fibrils were relatively similar (Fig. 6C). We noted also that
554 sonication of $M_i$ and purification by SEC did not produce any seed-competent species,
555 eliminating the possibility that small assemblies of sonication-induced fragments accounted
556 for seeding activity of $M_s$ (Fig. 6C). These experiments also indicated that it is not necessary
557 for tau monomer to be part of a fibril or to be exposed to sonication to produce an efficient
558 seed-competent monomer. Heparin, presumably by catalyzing a transition from an inert to a
559 seed-competent form, enables this critical conformational change.
560
561 **XL-MS reveals unique contacts associated with $M_s$**
562 To probe the structures of $M_i$ and $M_s$, we employed cross-linking with mass spectrometry (XL-
563 MS), which uses DSS-mediated crosslinking of proteins (monomer or larger assembly)
564 followed by trypsin proteolysis, enrichment of resultant fragments by SEC, and identification
565 by capillary liquid chromatography tandem mass spectrometry (MS). This method creates
566 restraints for structural models of single proteins or protein complexes[23,28,29]. We assigned
567 the complex fragment ion spectra to the corresponding peptide sequences using xQuest [24].
568 Denaturation of recombinant tau with 8M urea prior to crosslinking produced no
569 intramolecular cross-links (data not shown), indicating that crosslinks observed under native
570 conditions represented local structure. We studied $M_i$, fibril-derived $M_s$ and heparin-derived
571 $M_s$ using XLMS. Short reaction times ensured the production of only intra-molecular
572 crosslinks as monitored by SDS-PAGE (Fig. S6). XL-MS for each sample was carried out in
573 triplicate (Suppl. Table S1), and only considering consensus crosslinks present in each
574 replicate (Suppl. Table S2). $M_i$ exhibited crosslink patterns which indicated local and distant
575 intramolecular contacts (Fig. 7A). In $M_s$, we observed a consistent crosslinking of K150 with
576 K254, K267, K274 or K280 all located between RD 1 and 2. These crosslinks tracked

577 exclusively with $M_s$, both fibril- or heparin-derived (Fig. 7B,C). We never observed these
578 crosslinks in $M_i$. To test the relationship of this crosslink with seed function, we carried out
579 heat denaturation at 95°C for 3 or 24h, followed by XL-MS. Heating samples results in a
580 decrease in crosslink frequency (Fig. S7). Importantly, however, we observed a parallel
581 persistence of this crosslink pattern with seeding activity (Fig. 7B,C). The XL-MS results
582 indicate a distinct structure and seeding activity for $M_s$ that is surprisingly resistant to
583 denaturation at 95°C.
584
585 **AD brain contains $M_s$**
586 Given our experiments with recombinant $M_i$ and $M_s$, we wished to test whether similar
587 structures exist *in vivo*. We extracted AD and control brain samples using a dounce
588 homogenizer to avoid liberating significant monomer from fibrils. We immunoprecipitated tau
589 using an antibody that targets the amino-terminus (HJ8.5), and resolved the eluates by SEC,
590 followed by ELISA to determine tau levels (Fig. 8A,B). Tau from control brain purified in the
591 monomer fraction (Fig. 8A), while tau from AD brain distributed across multiple fractions,
592 corresponding to monomer and larger assemblies (Fig. 8B). When we tested each fraction for
593 seeding activity, we observed none in any control brain fraction (Fig. 8C). However, all AD
594 fractions contained seeding activity, including monomer (Fig. 8C). To exclude the possibility
595 that the brain homogenization protocol liberated $M_s$ from neurofibrillary tangles, we spiked tau
596 KO mouse brain samples with recombinant fibrils *in vitro*, or fibril-derived $M_s$. We then used
597 dounce homogenization and immuno-purification as for human brain. We evaluated the
598 seeding activity in total lysate, supernatant following 10,000 x g centrifugation, and SEC
599 fractions (Fig. 8D). We readily observed monomer seeding activity in tau KO brain spiked
600 with $M_s$, however we observed none in fractions that had been spiked with fibrils (Fig. 8D).
601 The homogenization protocol for human brain was thus unlikely to have liberated $M_s$ from
602 pre-existing tau fibrils.
603
604 To test for self-association of control-derived $M_i$ vs. AD-derived $M_s$, we purified these species
605 by SEC, and divided each monomer fraction in two. We snap-froze one fraction and
606 incubated the other overnight at room temperature. Then we again resolved the assemblies
607 via SEC and tested each fraction for seeding activity. Control monomer was inert, even after
608 incubation at RT (Fig. 8E). AD-derived $M_s$ that was purified, frozen, and re-purified by SEC
609 exhibited seeding activity exclusively in the monomer fraction (Fig. 8E). By contrast, AD-
610 derived $M_s$ incubated at RT formed seed-competent assemblies of increasing size (Fig. 8E).
611 We concluded that, as for other types of $M_s$, AD-derived $M_s$ exhibited an intrinsic capacity for
612 self-association into seed-competent assemblies. To compare structures of control vs. AD-
613 derived monomer via XL-MS, we isolated tau from brains of 3 AD patients and 3 age-
614 matched controls. In control-derived monomer, we observed no evidence of the crosslink that
615 marked $M_s$ (Fig. 8G). However, in each AD-derived $M_s$ sample we observed a discrete set of
616 crosslinks between aa150 and aa259-290 (Fig. 8H). This essential finding did not change, no
617 matter what method of homogenization we used (Supp. Fig. S8, Suppl. Table S3), and
618 implied a common structure that unifies ensembles of seed-competent tau monomer, whether
619 produced *in vitro* or *in vivo*.
620
621 **Models of seed-competent monomer suggest exposure of VQIINK and VQIVYK**
622 Based on intramolecular FRET and electron paramagnetic resonance spin labeling
623 Mandelkow et al. have previously proposed native tau structure to be in a "paperclip"
624 configuration, with the C-terminus folded over the RD[30]. To understand how core elements of
625 tau control its aggregation, we employed Rosetta to create models of tau structure for $M_i$ and

$M_s$ using restraints from the crosslink patterns and length of the DSS crosslinker. The overall energetics and radii of gyration in the models were comparable for $M_i$ and $M_s$ (Fig. S9), indicating global structural similarity. We thus focused on the RD, given its high frequency of intramolecular crosslinks, and primary role in aggregation (Fig. 9A). We observed differences in the predicted interface structure between R1/R2 and R2/R3 which encode two core VQIINK and VQIVYK motifs critical for tau amyloid formation[31,32]. The $M_i$ structural model predicted masking of VQIINK and VQIVYK sequences in compact "hairpin" structures (Fig. 9B, Supp. Movie $M_i$), similar to the structure of microtubule-bound tau previously determined by NMR [33]. By contrast, within $M_s$ the model predicted relative exposure of VQIINK and VQIVYK (Fig. 9C, Supp. Movie $M_s$). We next evaluated XL-MS-guided predictions of patient-derived tau, although lower sample quality and fewer high confidence crosslinks (possibly due to protein heterogeneity) limited our accuracy. As for recombinant protein, $M_i$ from control patients also featured VQIINK/VQIVYK sequences in a less accessible configuration (Fig. 9D, Supp. Table S1; Supp. Movie: Control1). In AD-derived $M_s$, long-range contacts from aa150 to R2 influenced the model, and predicted an exposed configuration of VQIINK/VQIVYK (Fig. 9E, Table S1; Supp. Movie: AD1). With important caveats, the models guided by XL-MS imply that the general difference between $M_i$ and $M_s$ derives from relative shielding vs. exposure of VQIINK/VQIVYK sequences.

**Limited proteolysis supports models of exposed VQIINK/VQIVYK sequences**

As an orthogonal comparison of the structures of $M_i$ and $M_s$, we used limited proteolysis with trypsin. $M_i$ or $M_s$ (heparin-exposed) that had been passed through a 100kD filter immediately prior were subjected to a fine time course of limited proteolysis (Fig. 10A). Each sample was prepared in triplicate with matched protein quantities to facilitate label-free analysis. We then used mass spectrometry to evaluate the production of tau fragments and mapped these to specific cleavage sites. We identified 60 peptides common across the two conditions (Suppl. Table S4). To summarize enrichment of peptides across the two datasets we compared the ratio of averaged kinetic profiles (Fig. S10). Differences between the $M_i$ and $M_s$ primarily localized to the RD (Fig. S10). In $M_i$, an R1R2 fragment was enriched (Fig. 10C) while only the R2 portion of that fragment was enriched in $M_s$ (Fig. 10D). We observed similar patterns in R2R3 (Fig. 10F,G). By contrast, other domains outside of these regions had similar cleavage kinetics in $M_i$ and $M_s$ (Fig. 10E,H, Fig. S10). Mapping these cleavage sites onto our structural models revealed that proteolysis in $M_i$ preferentially occurred outside the hairpin that includes VQIINK and VQIVYK amyloid sequences, while cleavage in $M_s$ occurred adjacent to the amyloid sequences (Fig. 10I,J). The cleavage patterns were thus consistent with structural models of VQIINK and VQIVYK regions, which predicted relative inaccessibility of hairpin-associated sequences in $M_i$, and accessibility in $M_s$.

## Discussion

We propose that tau monomer occupies two distinct and stable conformational ensembles. One set of structures (collectively termed $M_i$) is relatively inert, while another has intrinsic ability to self-assemble, and acts as a template, or seed, for fibril growth *in vitro* and in cells (collectively termed $M_s$). Multiple controls indicated that our original preparation of fibril-derived $M_s$ is in fact a monomer, uncontaminated by larger assemblies. Tau monomer purified from AD brain also had intrinsic seeding activity, and self-associated to produce larger seed-competent assemblies. A model restrained by the XL-MS data, and consistent with biochemical studies, predicts that VQIVYK and VQIINK sequences assume an open

675 configuration in all types of $M_s$ (fibril-derived, heparin-induced, and AD-derived). By contrast,
676 the model predicts lack of VQIINK/VQIVYK exposure in $M_i$. Limited proteolysis studies are
677 consistent with this idea, although clearly more detailed biochemical, biophysical, and
678 structural analyses will be needed to test its validity. Taken together, these data establish a
679 new concept for tau: this intrinsically disordered protein has multiple, stable monomeric
680 states, functionally distinguished by the presence or absence of seeding activity.
681
682 Amyloid proteins form progressively larger assemblies over time, and it has been difficult to
683 define the composition of the minimal seed. Mandelkow and colleagues studied tau
684 aggregation *in vitro* and concluded that a seed of 8-12 molecules existed in their
685 experimental system[4]. By contrast, Kuret and colleagues posited an "intermediate" of tau that
686 could subsequently initiate self-assembly, and their data, based on extrapolation of tau
687 concentrations needed to enable development of thioflavin fluorescence *in vitro*, were
688 consistent with a monomeric seed[1]. Wetzel and colleagues also proposed that a monomer is
689 the basis of a "thermodynamic nucleus" that templates the aggregation of synthetic
690 polyglutamine peptides[34]. However, no prior study has previously identified stable forms of
691 tau monomer that seed amyloid formation.
692
693 The actual cause of tau aggregation in tauopathies is unknown. It has been proposed that
694 dissociation of tau monomer from microtubules, possibly due to phosphorylation, allows high
695 concentration and self-association to form pathogenic assemblies[35]. In this study, using a
696 single source of recombinant protein, we define distinctly structured seed-competent and
697 inert forms of tau. We have similarly identified seed-competent species in human brain. In
698 reality "seed-competent" and "inert" forms of tau almost certainly represent multiple structural
699 ensembles separated by defined energy and/or kinetic barriers. The barrier for conversion of
700 an inert to a seed-competent form of tau can apparently be overcome by incubation with
701 heparin and/or incorporation into a fibril. In neurons, other factors such as post-translational
702 modifications and heterologous binding events likely play a role. Identification of the factors
703 that trigger conversion from inert to seed-competent forms will thus have obvious implications
704 for understanding disease mechanisms.
705
706 Isolation of seed-competent monomer from AD brain, with a very mild purification that
707 explicitly excludes sonication or vigorous tissue homogenization, strongly suggests that this
708 form of tau exists *in vivo*. Furthermore, we observed that both recombinant $M_s$ and AD-
709 derived $M_s$ build multimeric assemblies *in vitro* far more efficiently than $M_i$ or control-derived
710 monomer. Thus, we hypothesize that a uniquely structured form of tau may be required for
711 efficient assembly growth in cells. This contrasts with the idea that multimeric assemblies
712 uniquely stabilize the conformation of otherwise unstructured proteins as they incorporate into
713 the growing fibril, or that liquid-liquid phase separation with extremely high local concentration
714 underlies tau aggregation[36]. Instead, we imagine that the initiation of aggregation in human
715 brain might begin with a stable transition of tau monomer from an inert to a seed-competent
716 form. To fully study this process will require more extensive biochemical purification of tau $M_s$
717 from the earliest stages of disease.
718
719 $M_s$ has a remarkably stable structure, as it resists heat denaturation at 95°C for up to 3h. This
720 suggests a heretofore unrecognized conformation of tau that, to account for its slow
721 denaturation, likely involves multiple intra-molecular interactions involving short and long
722 range amino acid contacts. XL-MS provides some indication of what these might be, and
723 crosslinks between aa150 and R2 appear to mark a seed-competent conformation. In

agreement with the XL-MS results, we observed that heat inactivation of $M_s$ seeding activity occurs with a lag phase, rather than first order time-dependent decay. This implies a complex tertiary structure in which $M_s$ has multiple seed-competent intermediates. Future XL-MS studies performed at different temperatures could reveal these structures. With more advanced methods to interrogate the structure of monomeric tau in patient material, we imagine that "seed-competent monomer" will in fact represent myriad structures, depending on the underlying disease. This could provide an explanation for how a single tau protein might self-assemble into diverse amyloid strains. We note with excitement a recent study of the yeast prion Sup35 from the Tanaka laboratory. Like tau, Sup35 is intrinsically disordered, yet they have observed local structure that influences the conformations of fibrils it can form[37].

Without further studies to identify structures of tau at higher resolution, we cannot know for certain why one form acts as a seed and another does not. However, we gained important insights when we modeled the configurations of R1R2 and R2R3 using Rosetta, with crosslinks as restraints. With obvious caveats, our models predicted that the local environment surrounding two hexapeptide motifs, VQIINK and VQIVYK, which are required for tau to form amyloid structures, may explain the differences between seed-competent and inert forms. In the models of $M_i$, and control brain-derived tau, these motifs lie buried in hairpin structures. By contrast, in $M_s$ and AD-derived tau, both are exposed. VQIINK and VQIVYK thus might mediate intermolecular interaction in a growing assembly. In support of our structural model, the proteolysis experiments corroborate differences in exposure of the VQIINK and VQIVYK sequences in the R1R2 and R2R3 regions between $M_i$ and $M_s$. We note with great enthusiasm the recent study of Fitzpatrick et al. [38], which defined critical sequences of tau within the amyloid core that are based on VQIVYK and adjacent amino acids. Indeed, it has been recently observed that heparin binding involves residues spanning 270-290, and promotes expansion of the remainder of the molecule [39]. This is consistent with our predictions of relative exposure of VQIINK/VQIVYK. The diversity of exposed core elements (almost certainly beyond VQIINK/VQIVYK) could specify the formation of assemblies that give rise to distinct strains, as suggested by work from the Tanaka laboratory[37]. Consistent with this idea, the Fitzpatrick et al. study indicates that in AD-derived tau fibrils the VQIVYK sequence plays a key role in the core amyloid structure (along with adjacent amino acids), but the VQIINK sequence does not [38]. We also note that multiple disease-associated mutations in tau affect residues in close proximity to VQIINK/VQIVYK. For example, our models predict that serine or leucine substitutions at P301 (which cause dominantly inherited tauopathy) would uniquely destabilize the local structure and promote exposure of the VQIINK/VQIVYK sequences. Future experiments will test these ideas more definitively.

**Acknowledgements**

We thank Peter Davies for generously providing antibody reagents and ELISA protocol guidance. This work was supported by grants from the Tau Consortium and NIH grants awarded to 1R01NS071835 (M.I.D.), R01NS089932 (R.V.P. and M.I.D.), and the Effie Marie Cain Endowed Scholarship (L.A.J.). We appreciate the help of the Live Cell Imaging Core Facility administered by Katherine Luby-Phelps, Ph.D., and the Proteomics Core Facility at the University of Texas Southwestern Medical Center.

**Competing Interests**

772 A patent disclosure has been filed by H.M., L.A.J. and M.I.D. related to the use of unique
773 crosslinks to create biomarkers for neurodegenerative diseases.
774

775 **References**


776 1. Chirita CN, Congdon EE, Yin H, Kuret J. Triggers of full-length tau aggregation: a role
777 for partially folded intermediates. Biochemistry. 2005 Apr 19;44(15):5862–72.

778 2. Kar K, Jayaraman M, Sahoo B, Kodali R, Wetzel R. Critical nucleus size for disease-
779 related polyglutamine aggregation is repeat-length dependent. Nat. Struct. Mol. Biol.
780 2011 Mar;18(3):328–36. PMCID: PMC3075957

781 3. Ramachandran G, Udgaonkar JB. Mechanistic studies unravel the complexity inherent
782 in tau aggregation leading to Alzheimer's disease and the tauopathies. Biochemistry.
783 2013 Jun 18;52(24):4107–26.

784 4. Friedhoff P, Bergen von M, Mandelkow EM, Davies P, Mandelkow E. A nucleated
785 assembly mechanism of Alzheimer paired helical filaments. Proc. Natl. Acad. Sci.
786 U.S.A. National Academy of Sciences; 1998 Dec 22;95(26):15712–7. PMCID:
787 PMC28109

788 5. Neurodegenerative tauopathies. 2001;24(1):1121–59. Retrieved from:
789 http://www.annualreviews.org/doi/abs/10.1146/annurev.neuro.24.1.1121

790 6. Sanders DW, Kaufman SK, Holmes BB, Diamond MI. Prions and Protein Assemblies
791 that Convey Biological Information in Health and Disease. Neuron. Elsevier; 2016 Feb
792 3;89(3):433–48. PMCID: PMC4748384

793 7. Tau Trimers Are the Minimal Propagation Unit Spontaneously Internalized to Seed
794 Intracellular Aggregation. 2015 Jun 12;290(24):14893–903. PMCID: PMC4463437

795 8. Frost B, Jacks RL, Diamond MI. Propagation of tau misfolding from the outside to the
796 inside of a cell. J. Biol. Chem. American Society for Biochemistry and Molecular
797 Biology; 2009 May 8;284(19):12845–52. PMCID: PMC2676015

798 9. Holmes BB, Furman JL, Mahan TE, Yamasaki TR, Mirbaha H, Eades WC, et al.
799 Proteopathic tau seeding predicts tauopathy in vivo. Proc. Natl. Acad. Sci. U.S.A. 2014
800 Oct 14;111(41):E4376–85. PMCID: PMC4205609

801 10. Holmes BB, Devos SL, Kfoury N, Li M, Jacks R, Yanamandra K, et al. Heparan sulfate
802 proteoglycans mediate internalization and propagation of specific proteopathic seeds.
803 Proc. Natl. Acad. Sci. U.S.A. National Acad Sciences; 2013 Aug 13;110(33):E3138–47.
804 PMCID: PMC3746848

805 11. Sanders DW, Kaufman SK, Devos SL, Sharma AM, Mirbaha H, Li A, et al. Distinct Tau
806 Prion Strains Propagate in Cells and Mice and Define Different Tauopathies. Neuron.
807 2014 May 21. PMCID: PMC4171396

808 12. Furman JL, Holmes BB, Diamond MI. Sensitive Detection of Proteopathic Seeding
809 Activity with FRET Flow Cytometry. J Vis Exp. 2015;(106):e53205–5. PMCID:
810 PMC4692784

811 13. Goedert M, Jakes R, Spillantini MG, Hasegawa M, Smith MJ, Crowther RA. Assembly
812 of microtubule-associated protein tau into Alzheimer-like filaments induced by

813 sulphated glycosaminoglycans. Nature. Nature Publishing Group; 1996 Oct
814 10;383(6600):550–3.

815 14. Pérez M, Valpuesta JM, Medina M, Montejo de Garcini E, Avila J. Polymerization of tau
816 into filaments in the presence of heparin: the minimal sequence required for tau-tau
817 interaction. J. Neurochem. 1996 Sep;67(3):1183–90.

818 15. Frost B, Ollesch J, Wille H, Diamond MI. Conformational diversity of wild-type Tau
819 fibrils specified by templated conformation change. J. Biol. Chem. American Society for
820 Biochemistry and Molecular Biology; 2009 Feb 6;284(6):3546–51. PMCID:
821 PMC2635036

822 16. Acker CM, Forest SK, Zinkowski R, Davies P, d'Abramo C. Sensitive quantitative
823 assays for tau and phospho-tau in transgenic mouse models. Neurobiol. Aging. 2013
824 Jan;34(1):338–50. PMCID: PMC3474864

825 17. Measurement of microsecond dynamic motion in the intestinal fatty acid binding protein
826 by using fluorescence correlation spectroscopy. 2002 Oct 29;99(22):14171–6.
827 Retrieved from:
828 http://eutils.ncbi.nlm.nih.gov/entrez/eutils/elink.fcgi?dbfrom=pubmed&id=12381795&ret
829 mode=ref&cmd=prlinks

830 18. Spectroscopic Study and Evaluation of Red-Absorbing Fluorescent Dyes. 2003
831 Jan;14(1):195–204. Retrieved from: http://pubs.acs.org/doi/abs/10.1021/bc025600x

832 19. Morozova OA, March ZM, Robinson AS, Colby DW. Conformational features of tau
833 fibrils from Alzheimer's disease brain are faithfully propagated by unmodified
834 recombinant protein. Biochemistry. American Chemical Society; 2013 Oct
835 8;52(40):6960–7. PMCID: PMC4142060

836 20. Yanamandra K, Kfoury N, Jiang H, Mahan TE, Ma S, Maloney SE, et al. Anti-Tau
837 Antibodies that Block Tau Aggregate Seeding In Vitro Markedly Decrease Pathology
838 and Improve Cognition In Vivo. Neuron. 2013 Oct 16;80(2):402–14. PMCID:
839 PMC3924573

840 21. Laidler KJ. The development of the Arrhenius equation. Journal of Chemical Education.
841 1984.

842 22. Burnham KP, Anderson DR. Model selection and multimodal inference: a practical
843 information-theoretic approach. p. 61–3.

844 23. Leitner A, Joachimiak LA, Bracher A, Mönkemeyer L, Walzthoeni T, Chen B, et al. The
845 Molecular Architecture of the Eukaryotic Chaperonin TRiC/CCT. Structure. 2012
846 May;20(5):814–25.

847 24. Rinner O, Seebacher J, Walzthoeni T, Mueller LN, Beck M, Schmidt A, et al.
848 Identification of cross-linked peptides from large sequence databases. Nat. Methods.
849 Nature Publishing Group; 2008 Apr;5(4):315–8. PMCID: PMC2719781

850 25. Grimm M, Zimniak T, Kahraman A. xVis: a web server for the schematic visualization
851 and interpretation of crosslink-derived spatial restraints. Nucleic acids …. 2015.

852 26. Kahraman A, Herzog F, Leitner A, Rosenberger G, Aebersold R, Malmström L. Cross-
853 link guided molecular modeling with ROSETTA. Fernandez-Fuentes N, editor. PLoS
854 ONE. Public Library of Science; 2013;8(9):e73411. PMCID: PMC3775805

855 27. Lange OF, Rossi P, Sgourakis NG. Determination of solution structures of proteins up
856 to 40 kDa using CS-Rosetta with sparse NMR data from deuterated samples. 2012.

857 28. Lasker K, Förster F, Bohn S, Walzthoeni T, Villa E, Unverdorben P, et al. Molecular
858 architecture of the 26S proteasome holocomplex determined by an integrative
859 approach. Proc. Natl. Acad. Sci. U.S.A. National Acad Sciences; 2012 Jan
860 31;109(5):1380–7. PMCID: PMC3277140

861 29. Joachimiak LA, Walzthoeni T, Liu CW, Aebersold R, Frydman J. The structural basis of
862 substrate recognition by the eukaryotic chaperonin TRiC/CCT. Cell. 2014 Nov
863 20;159(5):1042–55. PMCID: PMC4298165

864 30. Jeganathan S, Bergen von M, Brutlach H, Steinhoff H-J, Mandelkow E. Global hairpin
865 folding of tau in solution. Biochemistry. 2006 Feb 21;45(7):2283–93.

866 31. Bergen von M, Friedhoff P, Biernat J, Heberle J, Mandelkow EM, Mandelkow E.
867 Assembly of tau protein into Alzheimer paired helical filaments depends on a local
868 sequence motif ((306)VQIVYK(311)) forming beta structure. Proc. Natl. Acad. Sci.
869 U.S.A. National Academy of Sciences; 2000 May 9;97(10):5129–34. PMCID:
870 PMC25793

871 32. Bergen von M, Barghorn S, Li L, Marx A, Biernat J, Mandelkow EM, et al. Mutations of
872 tau protein in frontotemporal dementia promote aggregation of paired helical filaments
873 by enhancing local beta-structure. J. Biol. Chem. 2001 Dec 21;276(51):48165–74.

874 33. Kadavath H, Jaremko M, Jaremko Ł, Biernat J, Mandelkow E, Zweckstetter M. Folding
875 of the Tau Protein on Microtubules. Angew. Chem. Int. Ed. Engl. WILEY-VCH Verlag;
876 2015 Aug 24;54(35):10347–51.

877 34. Bhattacharyya AM, Thakur AK, Wetzel R. polyglutamine aggregation nucleation:
878 thermodynamics of a highly unfavorable protein folding reaction. Proc. Natl. Acad. Sci.
879 U.S.A. 2005 Oct 25;102(43):15400–5. PMCID: PMC1266079

880 35. Mandelkow E-M, Mandelkow E. Biochemistry and cell biology of tau protein in
881 neurofibrillary degeneration. Cold Spring Harb Perspect Med. 2012 Jul;2(7):a006247–
882 7. PMCID: PMC3385935

883 36. Wegmann S, Eftekharzadeh B, Tepper K, Zoltowska KM, Bennett RE, Dujardin S, et al.
884 Tau protein liquid-liquid phase separation can initiate tau aggregation. EMBO J. 2018
885 Feb 22;:e98049.

886 37. Ohhashi Y, Yamaguchi Y, Kurahashi H, Kamatari YO, Sugiyama S, Uluca B, et al.
887 Molecular basis for diversification of yeast prion strain conformation. Proc. Natl. Acad.
888 Sci. U.S.A. National Academy of Sciences; 2018 Mar 6;115(10):2389–94.

889 38. Fitzpatrick AWP, Falcon B, He S, Murzin AG, Murshudov G, Garringer HJ, et al. Cryo-
890 EM structures of tau filaments from Alzheimer's disease. Nature. 2017 Jul 5;56:343.
891 PMCID: PMC5552202

892 39. Zhao J, Huvent I, Lippens G, Eliezer D, Zhang A, Li Q, et al. Glycan Determinants of
893 Heparin-Tau Interaction. Biophys. J. 2017 Mar 14;112(5):921–32. PMCID:
894 PMC5355497

895

896

897 FIGURE LEGENDS
898
899 **Figure 1: Seeding activity of tau monomer in cells and *in vitro***
900 (**A, B**) FL Cys-Tau(2A) was labeled with Alexa488 and resolved by SEC (**A**), or was fibrillized
901 in the presence of heparin, labeled with Alexa488, sonicated, and the assemblies resolved by
902 SEC (**B**). The column was calibrated using standards of the indicated hydrodynamic radii.
903 Color codes indicate the putative assembly units. (**C**) Tau assemblies were seeded into tau
904 RD-CFP/YFP biosensor cells. $M_i$ represents "inert" monomer purified in (A), which had no
905 seeding activity; $M_s$ represents "seed-competent" monomer purified in (B), which induced
906 intracellular tau aggregation. (**D**) FL WT tau and FL Cys-Tau(2A) were similarly fibrillized,
907 sonicated, and the fragments resolved by SEC. Seeding activity of each fraction was
908 determined. $M_s$ and larger assemblies of both forms of tau exhibited seeding activity, but not
909 $M_i$. IFD = Integrated FRET Density. (**E**) Tau assemblies of n=1,2,3 were passed through a
910 100kD size cutoff filter. Filtration had no effect on the $M_s$ fraction, whereas it reduced seeding
911 of assemblies of n=2 or 3. (**F**) Tau fibrils, trimer, or monomer were used to induce fibrillization
912 *in vitro* of full-length (0N4R) tau, measured by induced thioflavin fluorescence. $M_i$ had no
913 seeding activity, whereas $M_s$, trimer, and unfractionated fibrils had strong seeding activity.
914 (**G,H**) Titration of assemblies was performed. (**G**) $M_s$ exhibited an $EC_{50}$ of approximately
915 10nM (monomer equivalent); (**H**) Dimer and trimer had similar potencies. Concentration is
916 reflected as monomer equivalent.
917
918 **Figure 2: Analyses of $M_i$ and $M_s$ by CD and FCS**
919 (**A**) CD spectra of $M_i$ and $M_s$ were similar. (**B**) FCS Diffusion times for $M_i$, $M_S$, dimer, trimer,
920 and ~10mer, and the cross-correlation for $M_i$, $M_s$, dimer, trimer, and ≥10-mer were
921 determined after labeling of fibrils with Alexa488, or double labeling additionally with
922 tetramethylrhodamine prior to sonication. Table reflects the predicted diffusion time and the
923 actual diffusion time. The variance between predicted vs. observed times is reported. (**C-G**)
924 FCS for double-labeled tau assemblies. Cross correlation (CC) between the two dyes is
925 indicated in grey lines. (**H**) Summary of FCS cross-correlation, including free dyes. Neither
926 free dye, $M_i$ nor $M_s$ showed any cross-correlation, indicating that single species predominate.
927 All multimeric assemblies exhibited cross-correlation, indicating detection of both dyes within
928 a single particle.
929
930 **Figure 3: Fidelity of SEC purification of assemblies**
931 SEC fidelity was tested by isolating $M_s$ from fractions after fibril sonication. Remaining
932 fractions were combined with $M_i$, and the mix was re-isolated by SEC. In Group 1, after the
933 first isolation, the monomer fraction (which contains $M_s$) contained seeding activity. In Group
934 2, after the second purification by SEC, the monomer fraction (which contains $M_i$ spiked in)
935 did not exhibit seeding activity.
936
937 **Figure 4: Heat denaturation of assemblies**
938 (**A-C**) Heat-induced dissociation of assemblies. (**A**) The SEC fraction containing $M_s$ (B5) was
939 heated to 95°C for 3h and re-isolated by SEC prior to testing the FRET biosensor assay. No
940 loss in seeding activity was observed. (**B**) When the SEC fraction containing trimer (B8) was
941 heated similarly, seeding activity shifted to fractions that contain dimer and monomer (B7,
942 B5). (**C**) ~20-mer (A5) was largely stable to heating, although some smaller seed-competent
943 assemblies were liberated. (**D-G**) Various assemblies were subjected to heat denaturation at
944 the indicated temperatures and times, followed by analysis of seeding activity in the FRET
945 biosensor assay. Whereas ~10-mer and ~20-mer were relatively stable from 65-95°C,

946 monomer, dimer and trimer showed temperature-dependent loss of seeding activity. (**H**) Plot
947 of denaturation data for $M_s$ with multimodal regression curves superimposed.
948
949 **Figure 5: $M_s$ self-assembles**
950 $M_i$ and $M_s$ were incubated at 500nM or with equivalent amounts (monomer equivalent) of
951 dimer and trimer for various times prior to resolution by SEC. Assemblies were monitored by
952 reading the absorbance of fractions using micro BCA assay. (**A**) $M_i$ showed no self-
953 association. (**B**) $M_s$ exhibited self-association over time. (**C,D**) Dimer and trimer were stable
954 over time. (**E,F**) $M_i$ does not react with dimer or trimer to form larger assemblies. (**G,H**) $M_s$
955 reacts with dimer and trimer to form larger assemblies.
956
957 **Figure 6: Heparin induces transition from $M_i$ to $M_s$**
958 (**A**) Heparin treatment of FL WT tau was carried out for 15min, 1h, or 4h. Samples were
959 resolved by SEC, and fractions of various sizes were compared using the biosensor seeding
960 assay. "Pre-SEC" refers to the sample prior to fractionation. NT = monomer not treated with
961 heparin. At 15min, a small, but significant seeding activity was observed primarily in the
962 monomer fraction. By 1h this signal was very strong, and comparable to the signal of $M_s$
963 derived from sonicated fibrils. (**B**) $M_s$ derived from 4h heparin exposure was heated at 95°C
964 for different times, followed by analysis of seeding activity in the FRET biosensor assay.
965 Seeding activity decayed over 24h. (**C**) Seeding efficiencies per nM of tau (monomer
966 equivalent) of the various forms of $M_s$, sonicated, or unsonicated fibrils were relatively similar.
967 $M_i$ was sonicated identically to $M_s$, followed by purification via SEC, but exhibited no seeding
968 activity. Transfection of heparin failed to trigger intracellular aggregation (data not shown).
969
970 **Figure 7. Unique XL-MS patterns for different forms of $M_i$ and $M_s$**
971 Tau monomers were prepared as described, heated at 95°C for 0, 3 or 24h, reacted with
972 DSS, proteolyzed and analyzed by mass spectrometry to define intramolecular crosslinks.
973 Diagrams represent crosslinks within the tau protein. Tau is shown in grey; RD is colored in
974 red (R1), green (R2), blue (R3) and indigo (R4). Each diagram indicates only crosslinks
975 present in every triplicate (green or red). Crosslinks uniquely observed within $M_s$ preparations
976 are shown in red. Each sample was prepared, isolated by SEC, and then subjected XL-MS.
977 (**A**) $M_i$: tau monomer not previously fibrillized; (**B**) $M_s$: fibril-derived tau monomer; (**C**) $M_s$:
978 heparin-exposed tau monomer (0.25h or 1h). Crosslinks from aa150 to aa254-290 mark all
979 forms of $M_s$ after exposure to 95°C for 0h, 0.25h and 3h, but not 24h.
980
981 **Figure 8: AD brain contains seed-competent monomer**
982 Tau from control and AD brains was immunoprecipitated and subjected to SEC. (**A**) SEC
983 from control brain contained predominantly tau monomer. (**B**) SEC from AD brain contained a
984 range of tau assembly sizes. (**C**) Tau monomer from control brain exhibited no seeding
985 activity, whereas monomer from AD brain did, along with larger assemblies. Tau Unit refers
986 to the putative number of molecules per assembly. LF = Lipofectamine control. (**D**) Tau KO
987 mouse brain was spiked either with human tau $M_s$ or fibrils prior to dounce homogenization,
988 immunopurification, and resolution by SEC. Samples spiked with $M_s$ exhibited monomer
989 seeding activity, but not samples that had been spiked with fibrils. (**E**) AD-derived tau
990 monomer was incubated for the indicated times prior to SEC and determination of seeding
991 activity in each fraction. Larger seed-competent assemblies formed after 24h incubation at
992 RT. (**F, G**) Three control and AD brains were homogenized, monomer isolated, and evaluated
993 by XL-MS. Tau monomer from controls lacked the long-range crosslinks observed in $M_s$. AD-

994 derived $M_s$ contained long-range crosslinks (aa150 to aa254-290) also observed in
995 recombinant forms of $M_s$.
996
997 **Figure 9. Models of $M_i$ and $M_s$ suggest differences in the R1R2 and R2R3 regions**
998 XL-MS identified pairs were used as restraints in Rosetta to create structural models of
999 discrete tau domains. (**A**) Schematic highlighting the region of the RD encoding structural
000 differences between $M_i$ and $M_s$. Tau RD is colored in red (R1), green (R2), blue (R3) and
001 indigo (R4); N- and C-terminal portions of tau are shown in grey. Fragments of interest are
002 shown with their position in the RD. (**A**) recombinant $M_i$; (**B**) fibril-derived $M_s$, (**C**) Control $M_i$
003 and (**D**) AD-derived $M_s$. Regions surrounding the R1R2 and R2R3 are indicated, highlighting
004 two amyloid-forming sequences, VQIINK (green spheres) and VQIVYK (blue spheres). In
005 both forms of $M_i$ VQIINK and VQIVYK are associated with flanking amino acids in hairpin
006 structures. In both forms of $M_s$ the VQIINK and VQIVYK sequences are presented at the
007 protein surface. Please see Supplemental Movie files to better visualize the 3D orientation of
008 specific regions.
009
010 **Figure 10. Proteolysis of $M_i$ and $M_s$ reveals distinct patterns**
011 (**A**) $M_i$ and $M_s$ were prepared in triplicate, isolated by SEC, and passed through a 100kD filter
012 immediately prior to exposure to trypsin for 1, 5, 10, 30, 60 and 120min. Samples were
013 analyzed by mass spectrometry and kinetic profiles generated for peptides present at each
014 time point. (**B**) Tau RD is colored in red (R1), green (R2), blue (R3) and indigo (R4). Identified
015 peptides are shown with their position in the RD. (**C-H**) Kinetic profiles are indicated for
016 peptides that were more abundant in $M_i$ (**C, F**), $M_s$ (**D, G**) or equal in $M_i$ and $M_s$ (**E, H**). $M_i$ and
017 $M_s$ kinetic profiles are shown in blue and black, respectively. Fragments enriched in $M_i$ or $M_s$
018 were mapped onto corresponding regions in the structural models (**I, J**). The models are
019 shown as cartoons colored in red (R1), green (R2) and blue (R3). Cleavage sites are
020 indicated by arrows for $M_i$ (blue) and $M_s$ (black).
021
022 **Supplemental Table S1. Summary of triplicate XLMS datasets**
023
024 **Supplemental Table S2. Summary of consensus XLMS datasets**
025
026 **Supplemental Table S3. Summary of patient-derived XLMS datasets**
027
028 **Supplemental Table S4. Summary of peptides identified in the $M_i$ and $M_s$ proteolysis**
029
030 **Supplemental Movie Files**
031 PyMol was used to create rotating movies of all structural models for $M_i$ and $M_s$ derived from
032 recombinant or human sources. Each model of $M_s$ features one or both VQIINK/VQIVYK
033 sequences exposed. Forms of $M_i$ feature these sequences relatively buried in hairpin
034 structures.
035
036 **Supplemental Figure S6. SDS-PAGE of tau after sonication or heparin treatment.**
037 (**A**) Two different FL WT tau preparations were sonicated or not, and 1.5µg protein was then
038 resolved by SDS-PAGE and coomassie stain. Sonication induced a small degree of protein
039 fragmentation. (**B**) FL WT tau was exposed to heparin for 15min, sufficient to induce
040 conversion from $M_i$ to $M_s$, followed by DSS crosslinking for the indicated time periods. 100ng
041 Protein was then resolved by SDS-PAGE and silver stain. No small fragments or higher-order
042 crosslinked species were visible.

043
044 **Supplemental Figure S7. Frequency of crosslinks decrease with heat incubation**
045 Heat denaturation of $M_i$ and $M_s$ (fibril-derived and heparin treated for 0.25h, 1h) decreases
046 the abundance of consensus crosslink pairs (**A**). Columns represent data after exposure to
047 95°C for 0h, 3h and 24h.
048
049 **Supplemental Figure S8. Different brain homogenization methods yield similar**
050 **crosslink patterns**
051 A single AD brain sample was homogenized using four different methods: (**A**) Dounce
052 homogenization; (**B**) Pulse sonication; (**C**) Mechanical homogenization; (**D**) Mechanical
053 homogenization followed by pulse sonication. Diagrams represent crosslinks within the FL
054 tau protein. RD is colored in red (R1), green (R2), blue (R3) and indigo (R4). High confidence
055 XL-MS crosslinks are shown as light green lines; crosslinks found in $M_s$ are shown in red.
056
057 **Supplemental Figure S9. Energetics of Rosetta structural ensembles**
058 The ensembles are shown as a distribution of total energy of each model and radius of
059 gyration for recombinant $M_i$ (**A**), recombinant $M_s$ (**B**), control brain-derived $M_i$ (**C**) and AD-
060 derived $M_s$ (**D**).
061
062 **Supplemental Figure S10. Proteolysis reveals localized differences between $M_i$ and $M_s$**
063 The medians of the averaged kinetic profiles were compared as ratios for $M_i$ and $M_s$. The
064 data were compared to the mean (red line) and standard deviation (dotted grey line).
065 Peptides within the RD that are enriched in $M_i$ or $M_s$ are shown as colored dots according to
066 location in the RD and labeled with N-term and C-term peptide positions. As a reference the
067 tau RD is colored in red (R1), green (R2), blue (R3) and indigo (R4). Identified peptides are
068 shown with their position in the RD.

Figure 1

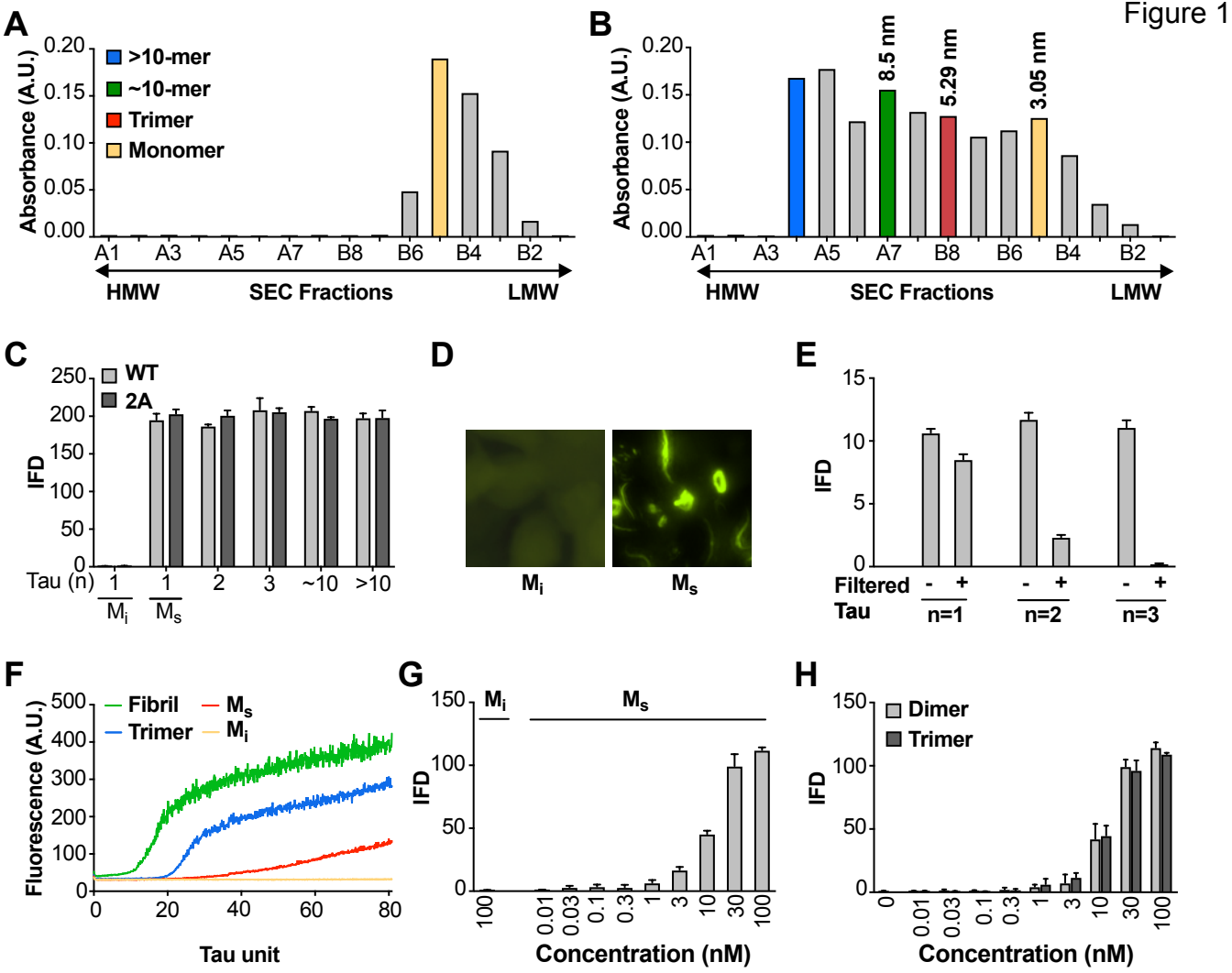
A
Absorbance (A.U.)
0.20
0.15
0.10
0.05
0.00
>10-mer
~10-mer
Trimer
Monomer
A1 A3 A5 A7 B8 B6 B4 B2
HMW
SEC Fractions
LMW
B
8.5 nm
5.29 nm
3.05 nm
C
WT
2A
IFD
250
200
150
100
50
0
Tau (n) 1 1 2 3 ~10 >10
Mi Ms
D
Mi
Ms
E
IFD
15
10
5
0
Filtered - + - + - +
Tau
n=1 n=2 n=3
F
Fibril
Trimer
Ms
Mi
Fluorescence (A.U.)
500
400
300
200
100
0
0 20 40 60 80
Tau unit
G
Mi
Ms
IFD
150
100
50
0
100 0.01 0.03 0.1 0.3 1 3 10 30 100
Concentration (nM)
H
Dimer
Trimer
IFD
150
100
50
0
0 0.01 0.03 0.1 0.3 1 3 10 30 100
Concentration (nM)

Figure 2

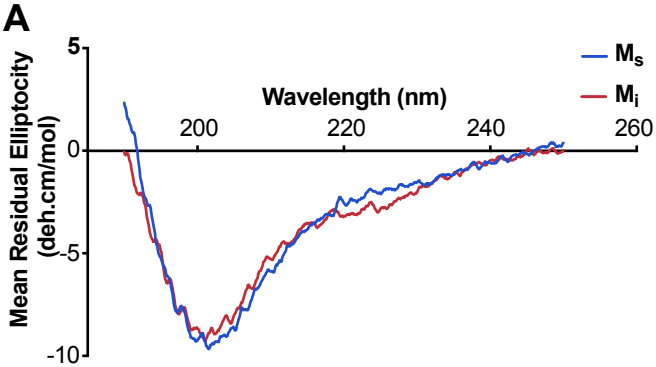


B

| Fraction | Units (n) | $T_{predicted}$ (μs) | $T_{actual}$ (μs) | Variance* |
|---|---|---|---|---|
| B5 | 1 | 210 | 211 | 0.005 |
| B7 | 2 | 264 | 270 | 0.022 |
| B8 | 3 | 303 | 309 | 0.020 |
| A7 | 10 | 452 | 561 | 0.241 |
| A4 | >10 | 518 | 1880 | 0.724 |

*Variance: 1-(Predicted / Actual Diffusion Time)

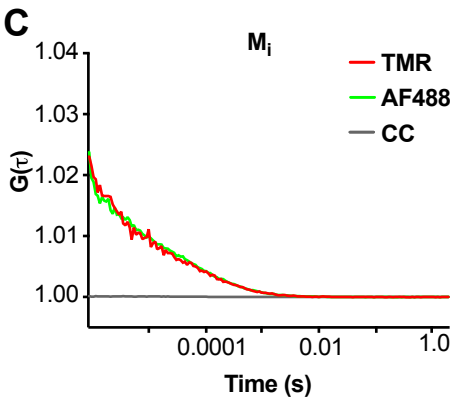


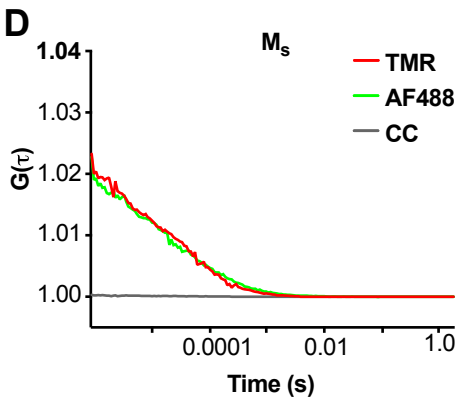


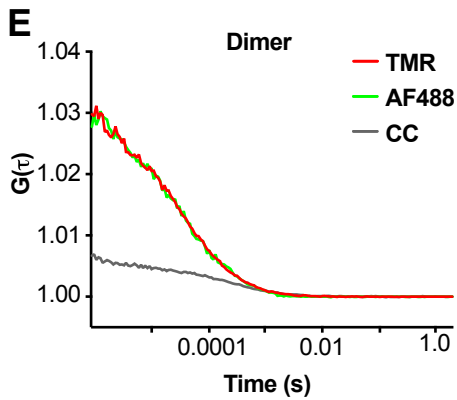


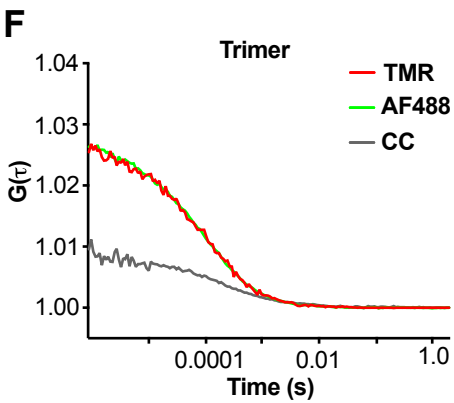


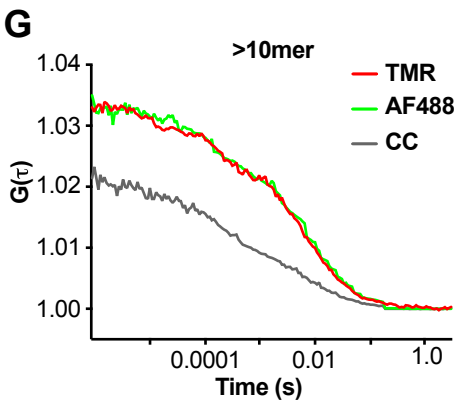


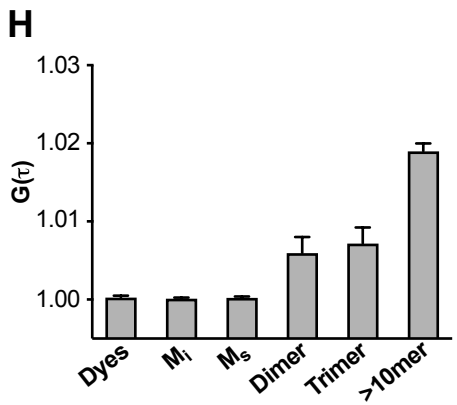

Figure 3

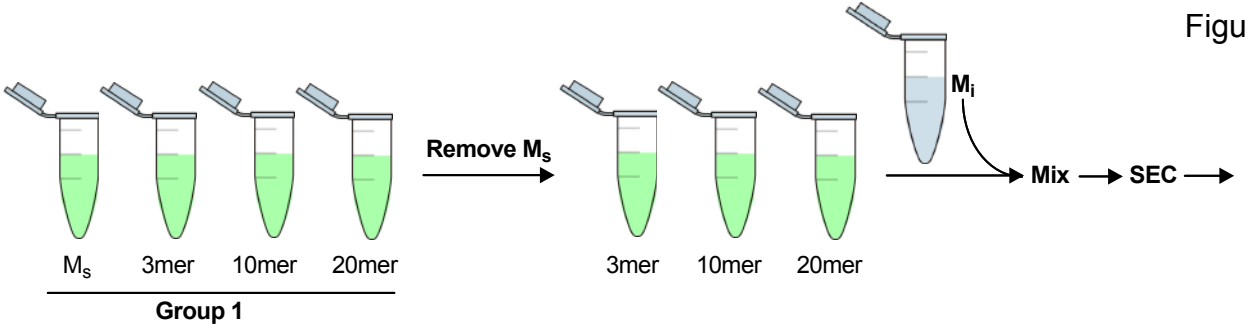
Remove $M_s$
$M_i$
Mix
SEC
$M_s$
3mer
10mer
20mer
Group 1
3mer
10mer
20mer

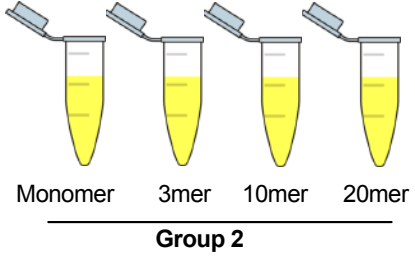
Monomer
3mer
10mer
20mer
Group 2

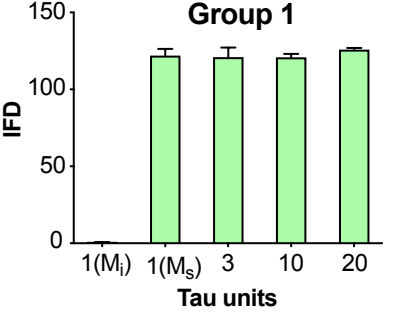
Group 1
IFD
150
100
50
0
1($M_i$)
1($M_s$)
3
10
20
Tau units

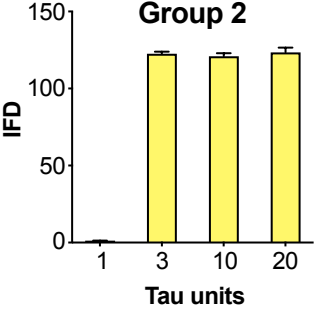
Group 2
IFD
150
100
50
0
1
3
10
20
Tau units

Figure 4

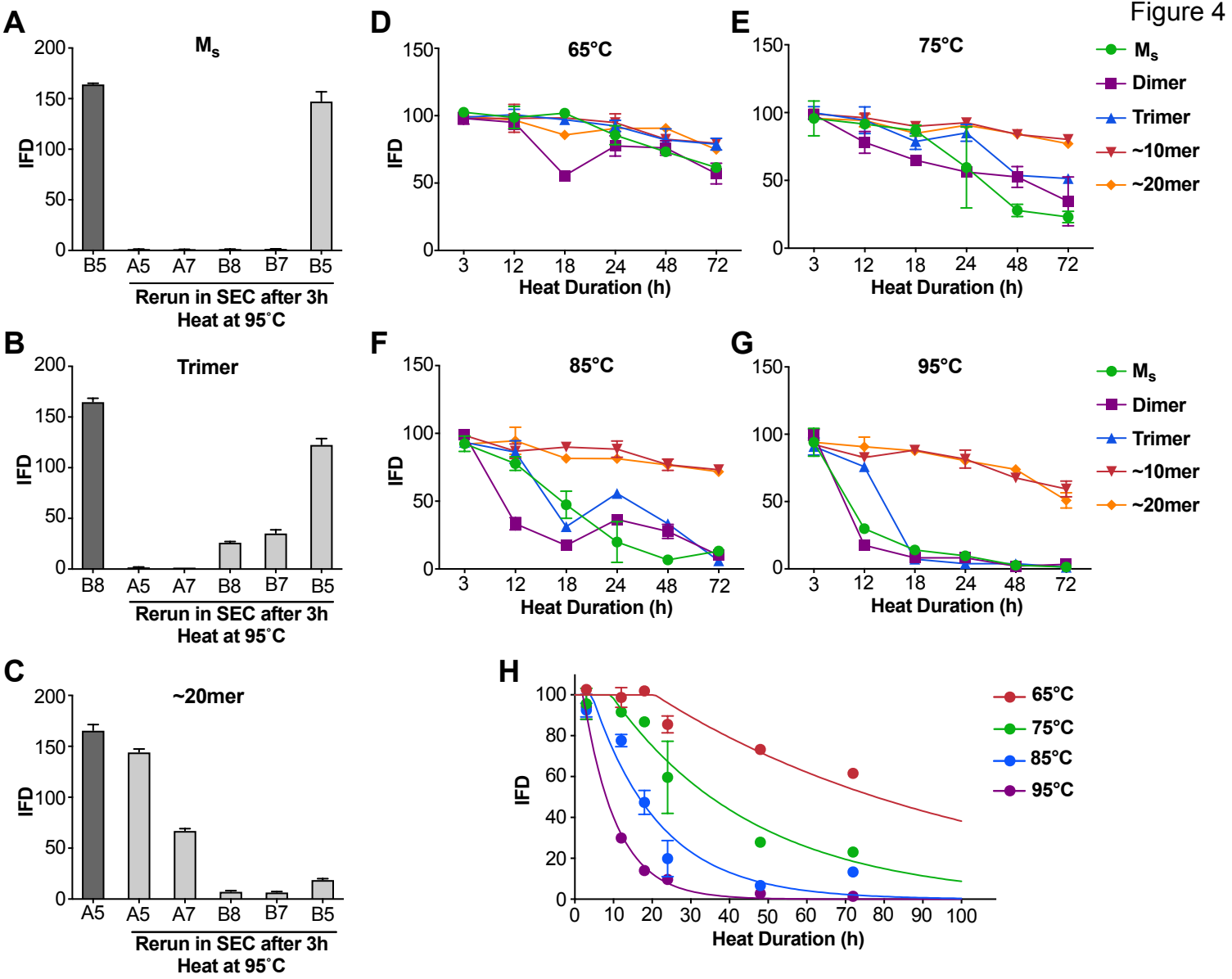
A
$M_s$
IFD
200
150
100
50
0
B5
A5
A7
B8
B7
B5
Rerun in SEC after 3h
Heat at 95˚C
B
Trimer
B8
A5
A7
B8
B7
B5
C
~20mer
A5
A5
A7
B8
B7
B5
D
65°C
E
75°C
F
85°C
G
95°C
3
12
18
24
48
72
Heat Duration (h)
$M_s$
Dimer
Trimer
~10mer
~20mer
H
65°C
75°C
85°C
95°C
0
10
20
30
40
50
60
70
80
90
100

Figure 5

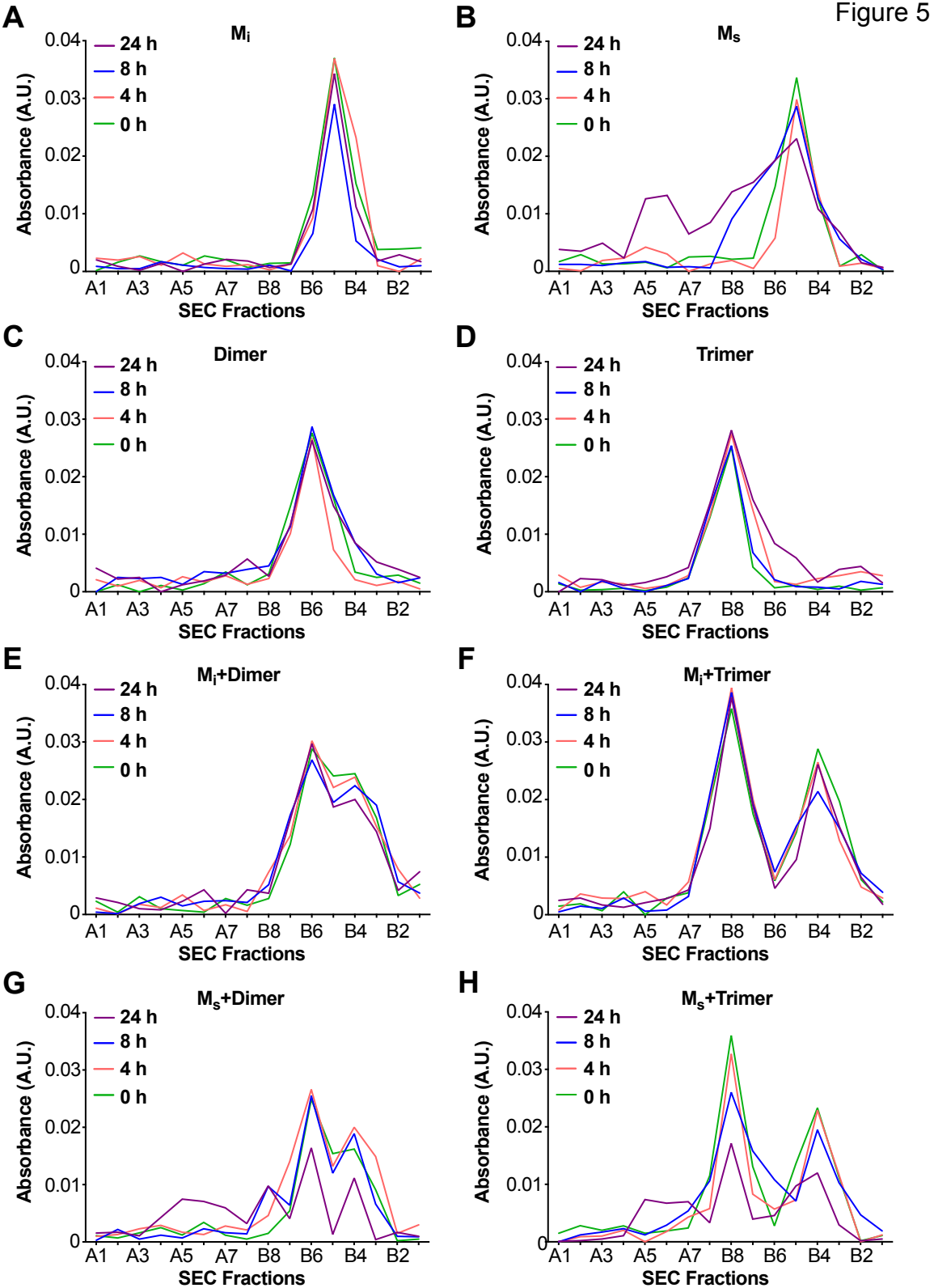
A
$M_i$
B
$M_s$
C
Dimer
D
Trimer
E
$M_i$+Dimer
F
$M_i$+Trimer
G
$M_s$+Dimer
H
$M_s$+Trimer
24 h
8 h
4 h
0 h
Absorbance (A.U.)
0.04
0.03
0.02
0.01
0
A1 A3 A5 A7 B8 B6 B4 B2
SEC Fractions

Figure 6

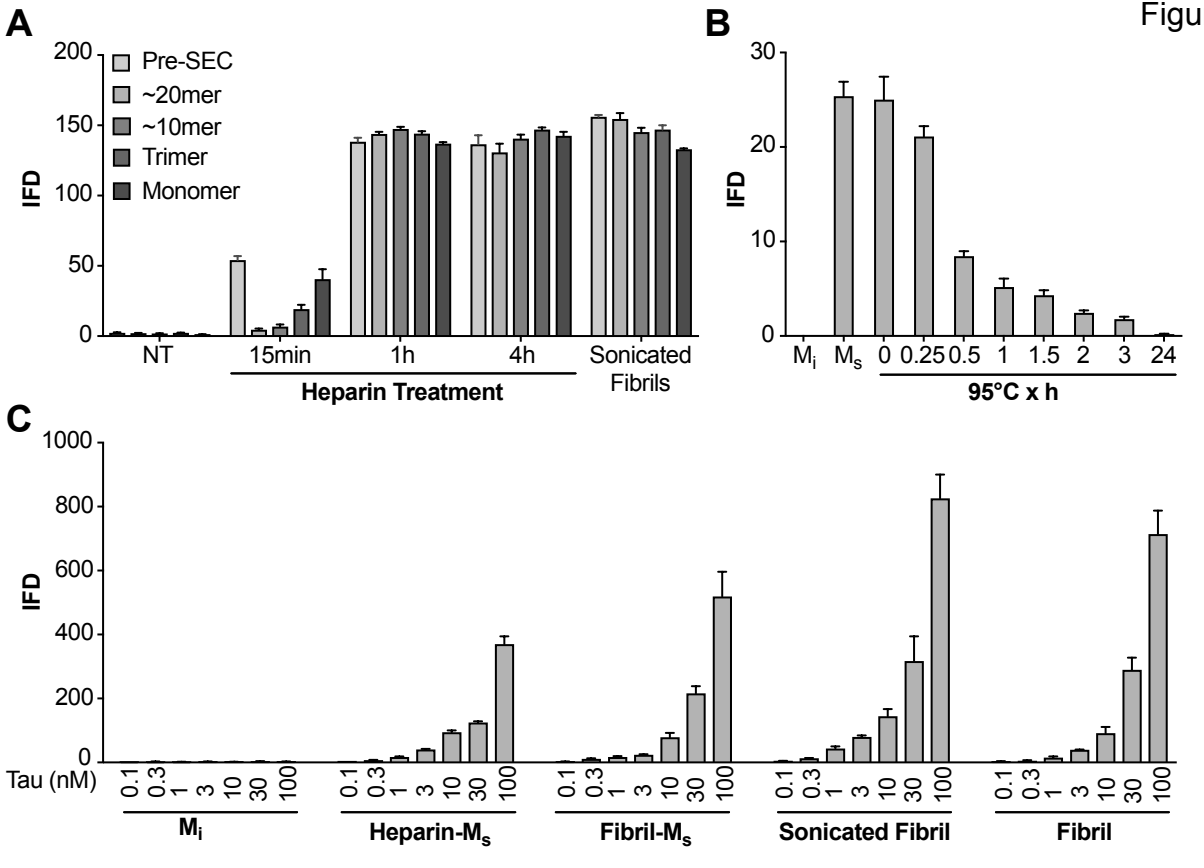
A
Pre-SEC
~20mer
~10mer
Trimer
Monomer
IFD
200
150
100
50
0
NT
15min
1h
4h
Sonicated Fibrils
Heparin Treatment
B
IFD
30
20
10
0
$M_i$
$M_s$
0
0.25
0.5
1
1.5
2
3
24
95°C x h
C
IFD
1000
800
600
400
200
0
Tau (nM)
0.1
0.3
1
3
10
30
100
$M_i$
Heparin-$M_s$
Fibril-$M_s$
Sonicated Fibril
Fibril

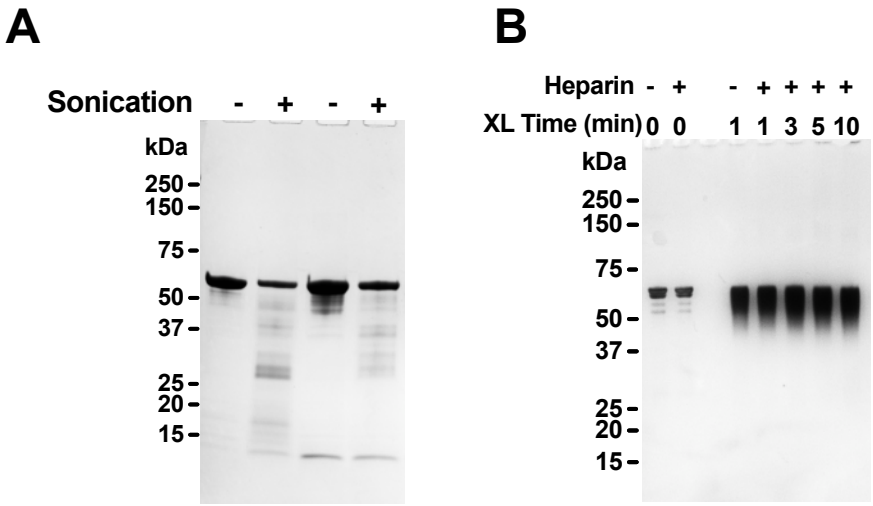
A
Sonication - + - +
kDa
250
150
75
50
37
25
20
15
B
Heparin - + - + + + +
XL Time (min) 0 0 1 1 3 5 10
kDa
250
150
75
50
37
25
20
15

Figure 7

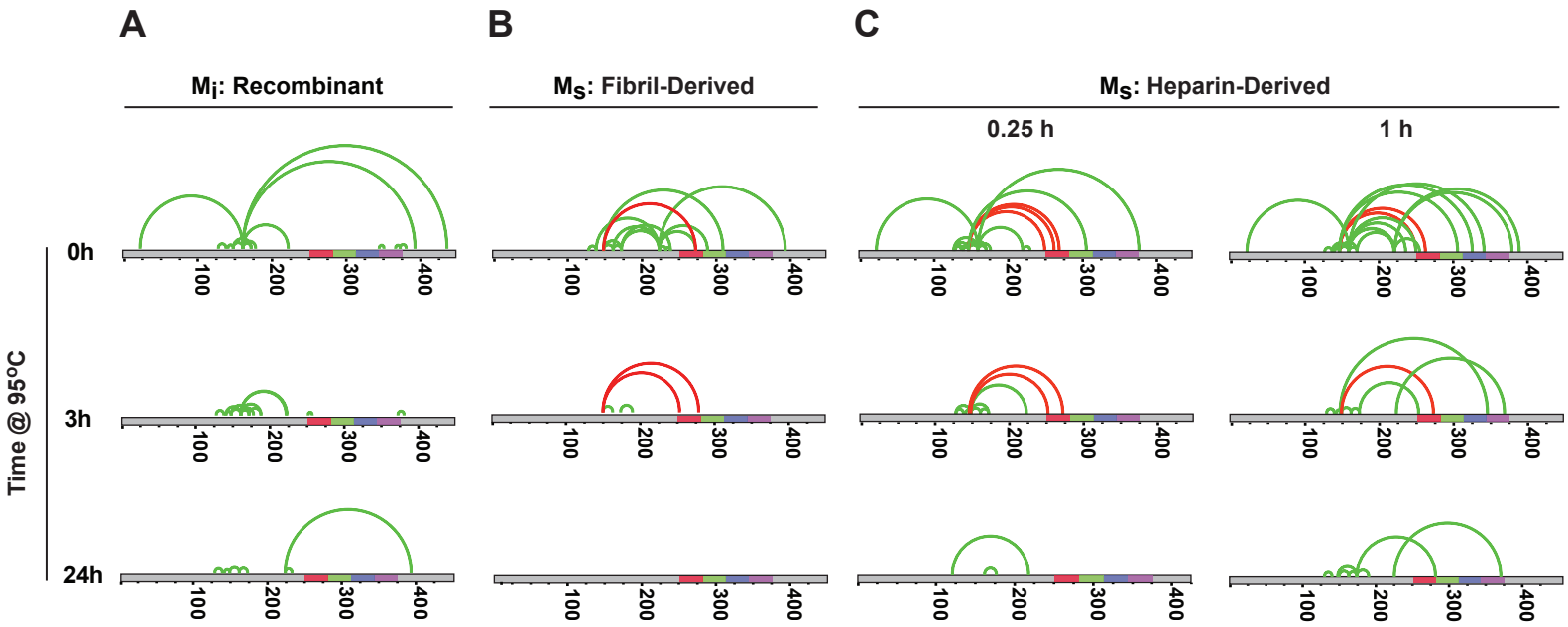
A
B
C
$M_i$: Recombinant
$M_S$: Fibril-Derived
$M_S$: Heparin-Derived
0.25 h
1 h
Time @ 95°C
0h
3h
24h
100
200
300
400

Supplemental Figure 7

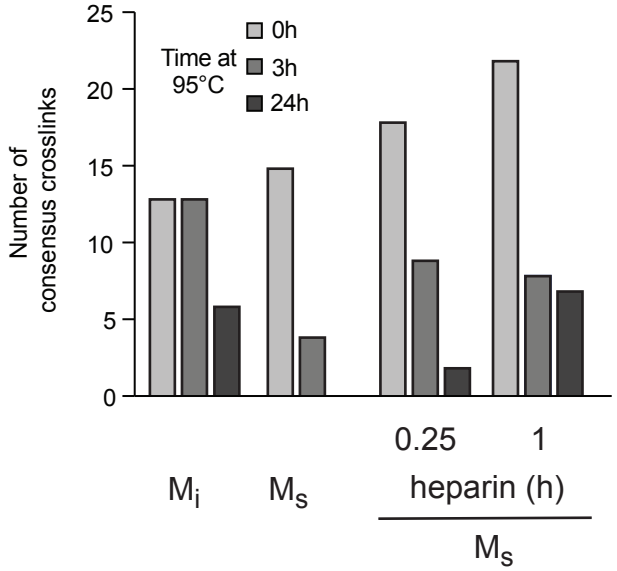

Figure 8

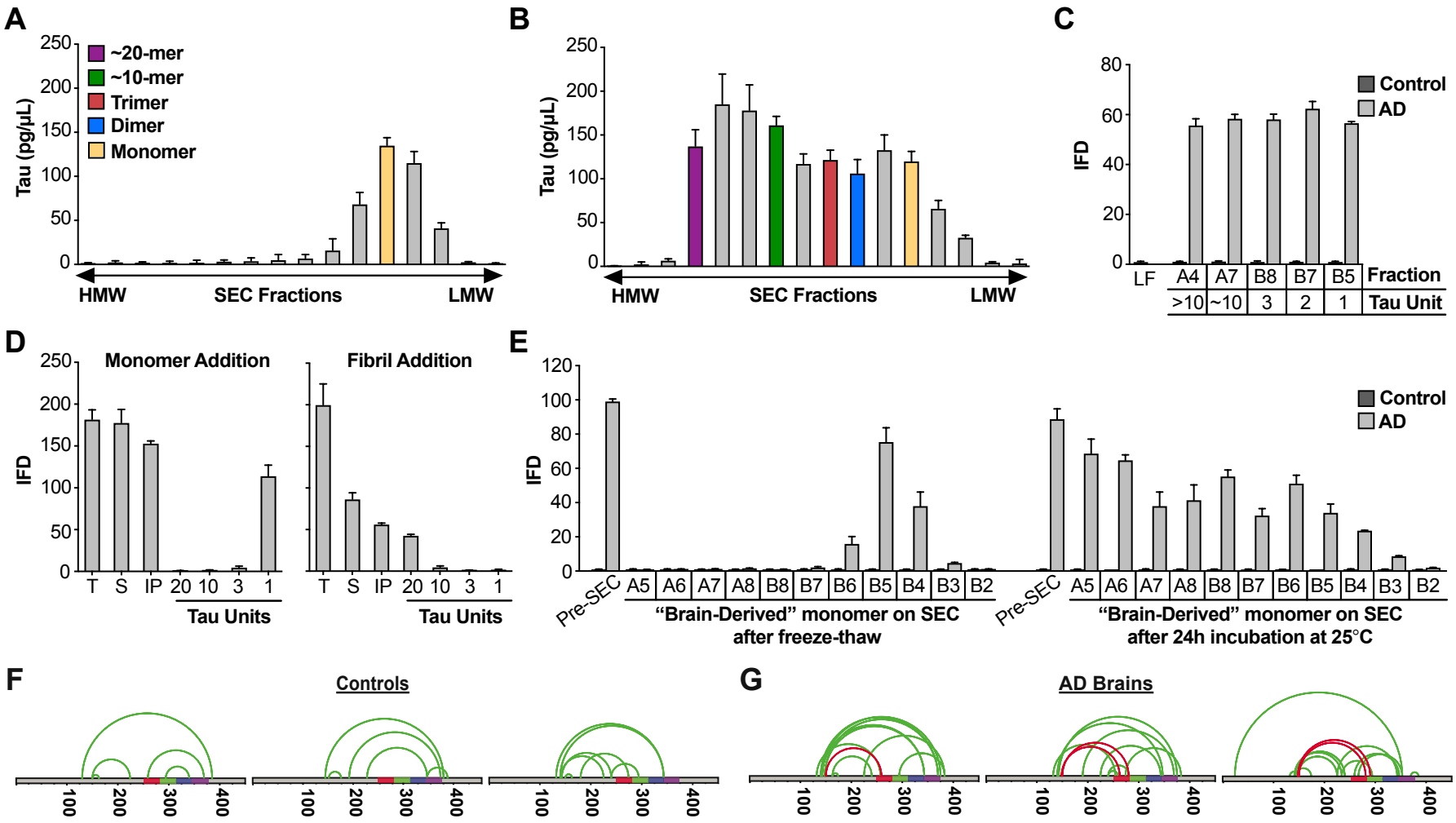
A
~20-mer
~10-mer
Trimer
Dimer
Monomer
Tau (pg/µL)
HMW
SEC Fractions
LMW
B
Tau (pg/µL)
HMW
SEC Fractions
LMW
C
Control
AD
IFD
LF
A4 A7 B8 B7 B5 Fraction
>10 ~10 3 2 1 Tau Unit
D
Monomer Addition
Fibril Addition
IFD
T S IP 20 10 3 1
Tau Units
E
Control
AD
IFD
Pre-SEC A5 A6 A7 A8 B8 B7 B6 B5 B4 B3 B2
"Brain-Derived" monomer on SEC after freeze-thaw
"Brain-Derived" monomer on SEC after 24h incubation at 25°C
F
Controls
G
AD Brains
100 200 300 400

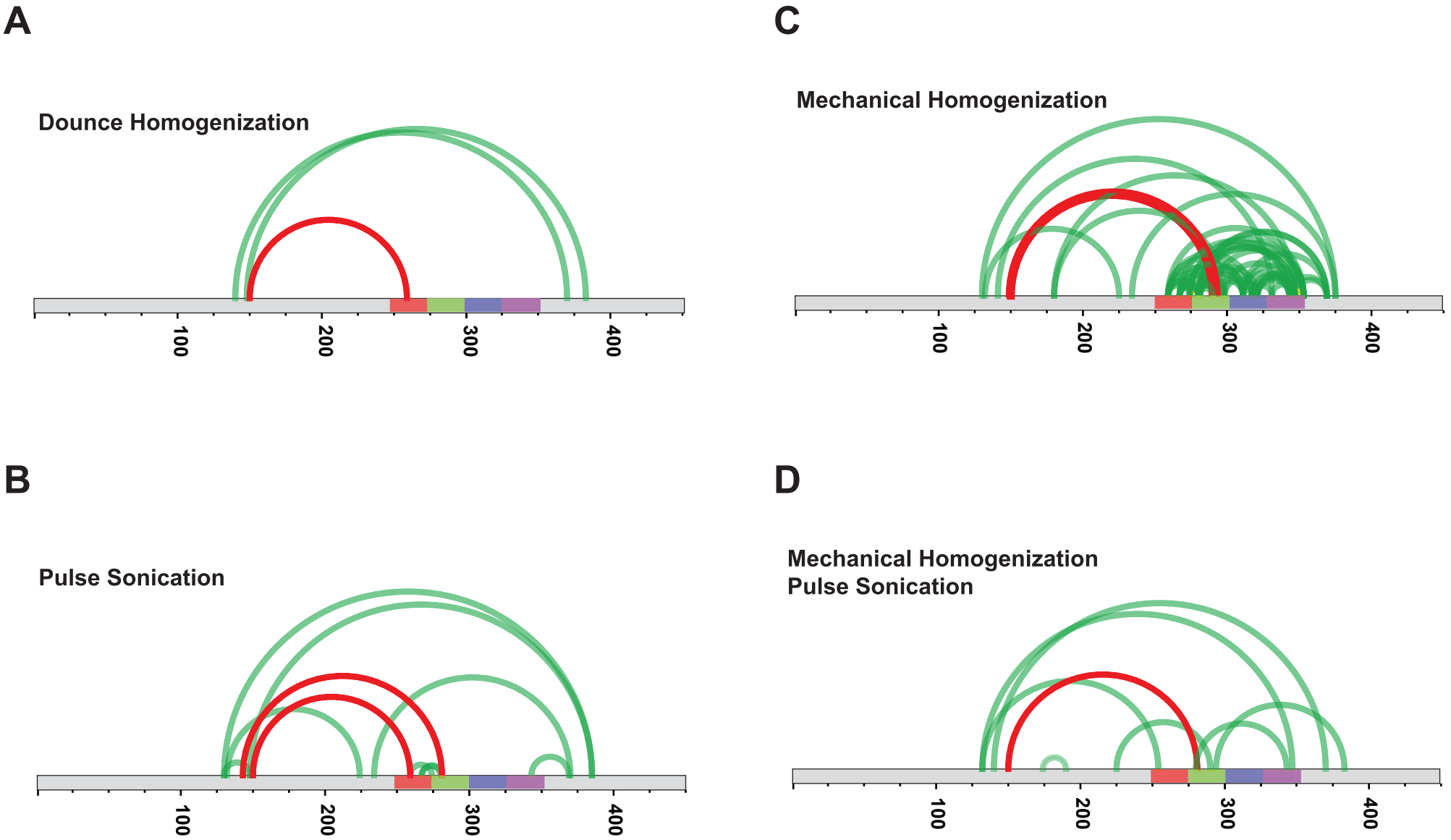
A
Dounce Homogenization
100
200
300
400
C
Mechanical Homogenization
100
200
300
400
B
Pulse Sonication
100
200
300
400
D
Mechanical Homogenization
Pulse Sonication
100
200
300
400

Figure 9

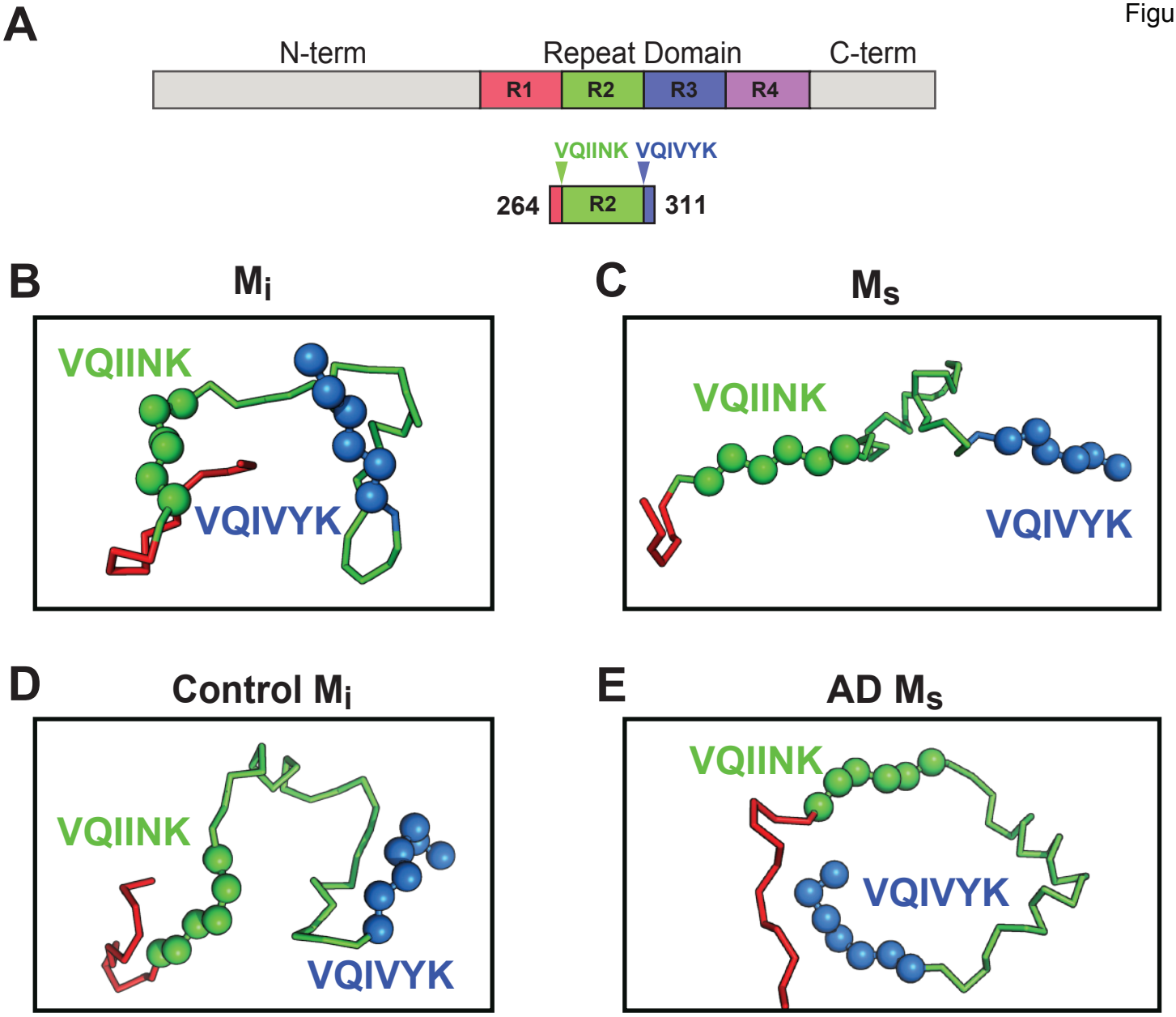
A
N-term
Repeat Domain
C-term
R1
R2
R3
R4
VQIINK
VQIVYK
264
R2
311
B
Mi
VQIINK
VQIVYK
C
Ms
VQIINK
VQIVYK
D
Control Mi
VQIINK
VQIVYK
E
AD Ms
VQIINK
VQIVYK

Supplemental Figure 9

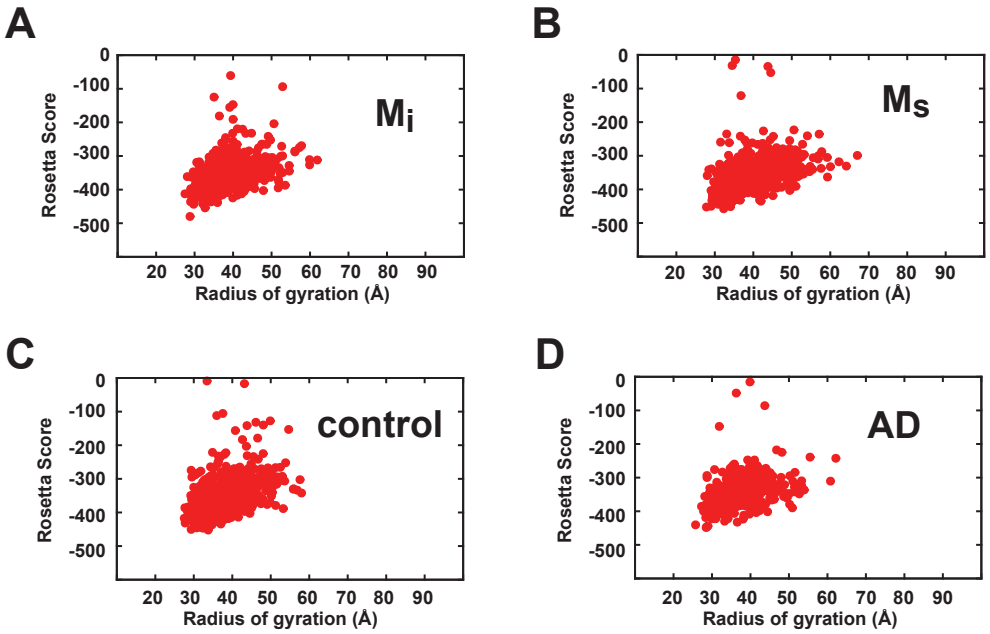

Figure 10

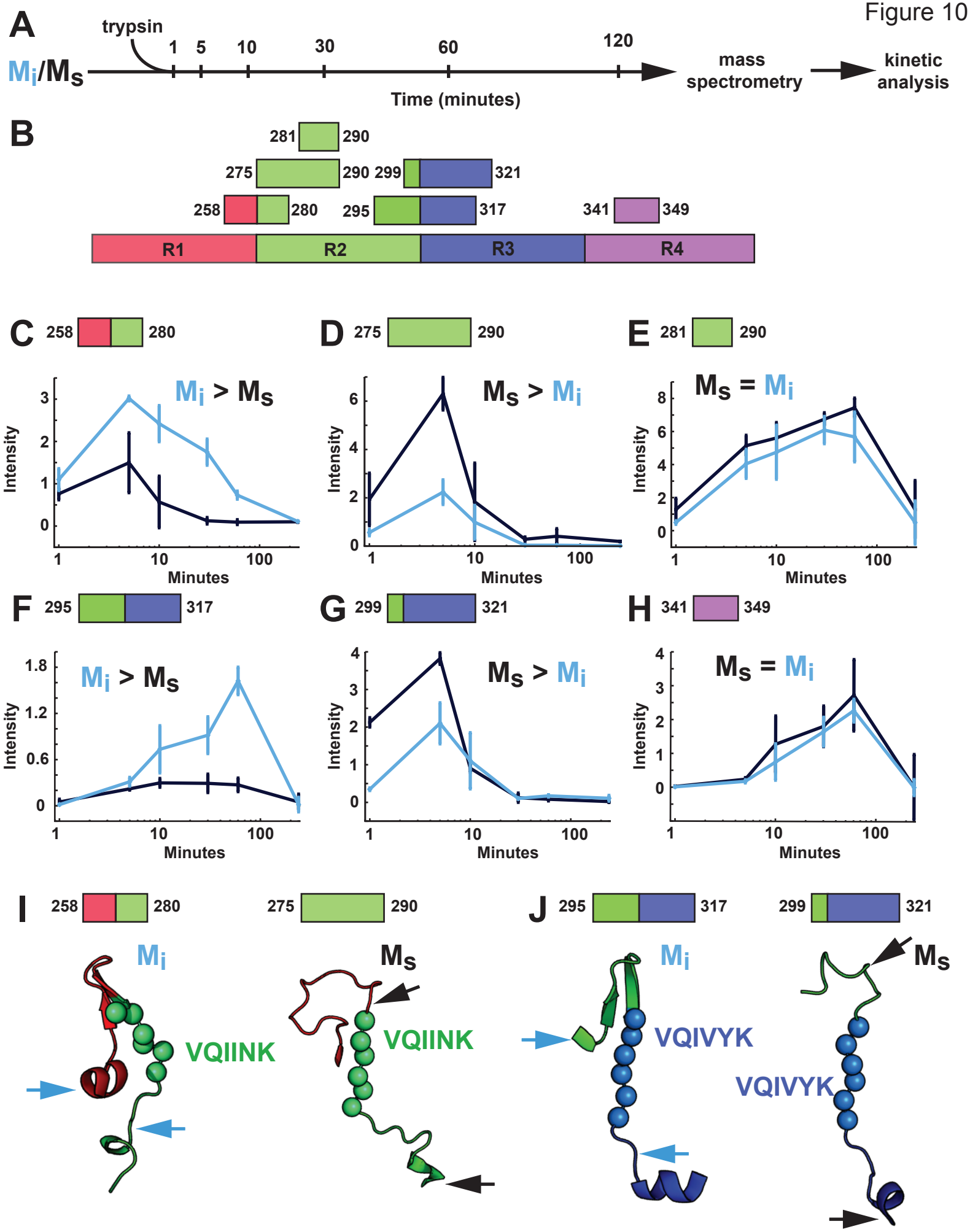
A
trypsin
Mi/Ms
1 5 10 30 60 120
Time (minutes)
mass spectrometry
kinetic analysis
B
281 290
275 290 299 321
258 280 295 317 341 349
R1 R2 R3 R4
C 258 280
Mi > Ms
Intensity
Minutes
D 275 290
Ms > Mi
E 281 290
Ms = Mi
F 295 317
Mi > Ms
G 299 321
Ms > Mi
H 341 349
Ms = Mi
I 258 280 275 290
Mi
Ms
VQIINK
VQIINK
J 295 317 299 321
Mi
Ms
VQIVYK
VQIVYK
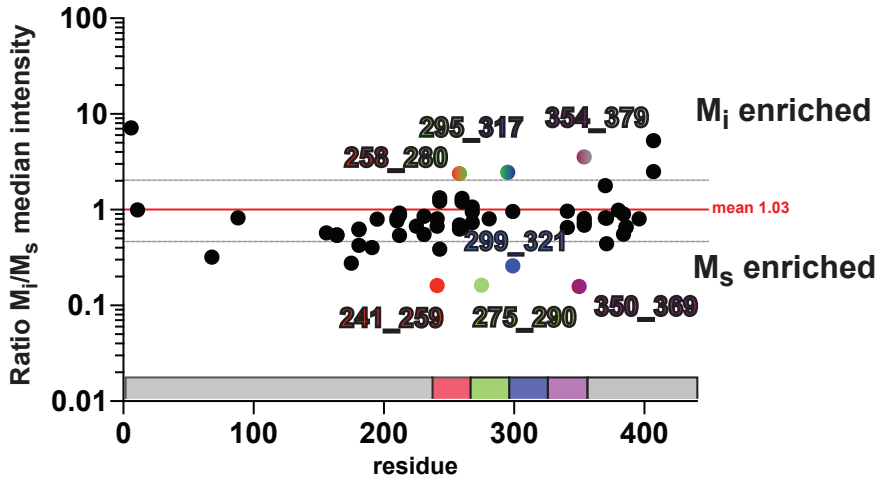
Supplemental Figure 10